

OPTICAL WAVELET TRANSFORM
USING WAVELENGTH MULTIPLEXING

Miss Chanita Kaewprasert

A Thesis Submitted in Partial Fulfillment of the Requirements
for the Degree of Master of Science in Laser Technology and Photonics
Suranaree University of Technology
Academic Year 1999
ISBN 974-7359-53-7

การแปลงออฟติคอลลเวฟเล็ตโดยการใช้มัลติเพิล็กซ์ความยาวคลื่น

นางสาวชนิตา แก้วประเสริฐ

วิทยานิพนธ์นี้เป็นส่วนหนึ่งของการศึกษาตามหลักสูตรปริญญาวิทยาศาสตรมหาบัณฑิต

สาขาวิชาเทคโนโลยีเลเซอร์และโฟตอนิกส์

มหาวิทยาลัยเทคโนโลยีสุรนารี

ปีการศึกษา 2542

ISBN 974-7359-53-7

Thesis Title

Optical Wavelet Transform Using Wavelength Multiplexing

Suranaree University of Technology Council has approved this thesis
submitted in partial fulfillment of the requirements for a Master's Degree

Thesis Examining Committee

.....
(Asst. Prof. Dr. Joewono Widjaja)
Chairman

.....
(Asst. Prof. Dr. Joewono Widjaja)
Thesis Advisor

.....
(Prof. Dr. Vutthi Bhanthumnavin)
Committee Member

.....
(Asst. Prof. Dr. Arjuna Chaiyasena)
Committee Member

.....
(Assoc. Prof. Dr. Kasem Prabripataloong)
Vice Rector for Academic Affairs

.....
(Assoc. Prof. Dr. Tassanee Sukosol)
Dean, Institute of Science

นางสาวชนิตา แก้วประเสริฐ: การแปลงออฟติคอลลูว์เล็ทโดยการใช่มัลติเพล็กซ์ความยาวคลื่น
(OPTICAL WAVELET TRANSFORM USING WAVELENGTH MULTIPLEXING)

อ. ที่ปรึกษา: ผศ. ดร. ยูโวจิน วิจิตยา, 64 หน้า. ISBN 974-7359-53-7

วิทยานิพนธ์นี้ศึกษาวิธีการแบบใหม่ ในการสร้างการแปลงออฟติคอลลูว์เล็ทแบบ 2 มิติ โดยใช่มัลติเพล็กซ์ความยาวคลื่น วิธีการที่นำเสนอใช้เกรตติงเพื่อสร้างรูปภาพหลายภาพ และใช้ฟูรีเยร์ออฟติค โดยสเปคตรัมของวัตถุที่อยู่ ณ ตำแหน่งหน้าเลนส์เป็นระยะทางเท่ากับความยาวโฟกัสของเลนส์ จะทำให้เกิดขึ้นที่ตำแหน่งหลังเลนส์เป็นระยะทางเท่ากับระยะโฟกัสของเลนส์ และขนาดของสเปคตรัมนั้นจะแปรผกผันกับความยาวคลื่นของแสงที่ฉายจากแหล่งกำเนิด ในการสร้างทางออฟติค ระบบจะถูกสร้างโดยการต่อชุดอุปกรณ์ทางแสง 4-f 2 ชุด ขนานกัน ซึ่งส่วนแรกของชุดอุปกรณ์จะทำให้เกิดรูปภาพของอินพุทหลายภาพเพื่อจะใช้ในการวิเคราะห์ ในขณะที่ส่วนที่สองสร้างการแปลงเวฟเล็ทแบบหลายช่องสัญญาณบนผลของส่วนแรก โดยใช้ออร์เล็ทเวฟเล็ท ผลการทดลอง และการจำลองโดยคอมพิวเตอร์ รวมทั้งการวิเคราะห์สัคยภาพของระบบได้ถูกนำเสนอ ผลลัพธ์แสดงว่าวิธีการที่นำเสนอสามารถใช้ได้ตามทฤษฎี

สาขาวิชาเทคโนโลยีเลเซอร์และโฟโตนิกส์ ลายมือชื่อนักศึกษา..... *ชนิตา แก้วประเสริฐ*

ปีการศึกษา 2542 ลายมือชื่ออาจารย์ที่ปรึกษา..... *[ลายมือ]*

ลายมือชื่ออาจารย์ที่ปรึกษาร่วม..... *[ลายมือ]*

ลายมือชื่ออาจารย์ที่ปรึกษาร่วม..... *[ลายมือ]*

MISS CHANITA KAEWPRASERT: OPTICAL WAVELET TRANSFORM
 USING WAVELENGTH MULTIPLEXING THESIS ADVISOR: ASST.
 PROF. DR. JOEWONO WIDJAJA, Ph. D. 64 PP. ISBN 974-7359-53-7

This thesis studies a new method to implement the multi-channel two dimensional (2-D) optical wavelet transform by using wavelength multiplexing. The proposed method uses grating to produce multiple images and takes an advantage of the Fourier optics, where a spectrum of an object scene placed at the front focal plane of a lens could be obtained at the back focal plane with its spatial size inversely proportional to the wavelength of the illuminating light source. In its optical implementation, the system is constructed by cascading two 4-f optical setups where the first setup produces multiple images of the input scene to be analyzed, while the second one performs multi-channel wavelet transformations by using the Morlet wavelet. Experimental results and computer simulations together with the analysis of the system performance are presented. The results show that the proposed method could work in a good agreement with the theory.

สาขาวิชาเทคโนโลยีเลเซอร์และโฟโตนิกส์

ปีการศึกษา 2542

ลายมือชื่อนักศึกษา.....*ชัญฉา แก้วประเสริฐ*.....

ลายมือชื่ออาจารย์ที่ปรึกษา.....*[Signature]*.....

ลายมือชื่ออาจารย์ที่ปรึกษาร่วม.....*[Signature]*.....

ลายมือชื่ออาจารย์ที่ปรึกษาร่วม.....*[Signature]*.....

ACKNOWLEDGMENTS

I wish to express my deepest gratitude to thesis advisor, Asst. Prof. Dr. Joewono Widjaja, for his continuous guidance, support, constructive comments, and encouragement throughout the course of my study as well as his corrections of the manuscript revising manuscript. His kindness will always be remembered.

This study would not have been possible without equipment and instruments were kindly provided by Professor Dr. Vutthi Bantumnavin. The slide holders constructed by Mr. Komsun Pasayadej, the engineer at the Center of Science and Technological Equipment are highly appreciated.

I would like also to extend my appreciation to the thesis committee members, Prof. Dr. Vutthi Bantumnavin, Asst. Prof. Dr. Eckart Schulz, and Asst. Prof. Dr. Arjuna Chaiyasena.

Finally, I am most grateful to my parents and Mr. Akarapol Chirdchoo for their continuous encouragement, constant care and assistance during the course of this study.

Miss Chanita Kaewprasert

CONTENTS

	Page
Thai abstract.....	IV
English abstract.....	V
Acknowledgement.....	VI
Contents.....	VII
List of Tables.....	IX
List of Figures.....	X
Chapter I. Introduction.....	1
1.1 Introduction.....	1
1.2 Historical review.....	1
1.3 Purpose of the thesis.....	3
1.4 Hypothesis.....	4
1.5 Organization of the thesis.....	4
Chapter II Wavelet Transform.....	6
2.1 Why the wavelet transform ?.....	6
2.2 Definition of the wavelet transform.....	11
2.3 The Morlet wavelet.....	13
Chapter III. Fourier Optics.....	15
3.1 Introduction.....	15
3.2 Fourier Analysis in twodimensions.....	16

CONTENTS (CONTINUED)

	Page
3.2.2 Fourier analysis in two dimensions.....	16
3.3 The Huygens-Fresnel principle and diffraction theory.....	20
3.4 Fourier transform properties of lenses.....	24
3.4.1 The thin lens as phase transformation.....	24
3.4.2 The thickness function.....	26
3.4.3 The paraxial approximation.....	28
3.4.4 Phase transformation and its physical meaning.....	28
3.4.5 Fourier transformation by a positive lens.....	30
3.5 Coherent optical processing system with spatial filtering.....	34
Chapter IV. Multi-channel 2-D WT.....	37
4.1 Introduction.....	37
4.2 Multi-channel 2-D optical WT by using wavelength multiplexing.....	38
4.2.1 Generating the multi-channel images by 2-D gratings.....	38
4.2.2 Multi-channel WT by using wavelength multiplexing.....	41
4.3 Experimental setup.....	43
4.4 Experimental results.....	48
4.5 Computer simulation.....	52
4.6 System performance.....	56
Chapter V. Conclusion.....	59
References.....	61
Biography.....	64

LIST OF TABLES

Table	Page
2.1 Morlet wavelet and its spectrum.....	14
4.1 The pass band of the wavelet filter.....	46

LIST OF FIGURES

Figure	Page
2.1 Relationship between the FT and its inverse FT.....	7
2.2 A stationary cosine signal and its spectrum.....	8
2.3 A non-stationary cosine signal and its spectrum.....	8
2.4 Time-frequency plane of STFT.....	11
2.5 Time-frequency plane of WT.....	11
3.1 Diffraction geometry.....	20
3.2 The thickness function.....	25
3.3 Calculation of the thickness function.....	27
3.4 Effects of a converging and a diverging lens on a normally incident plane wave.....	30
3.5 The geometry for performing the Fourier transform by a positive thin lens.....	31
3.6 A coherent optical information processing system.....	36
4.1 Two cascaded 4-f optical setup.....	38
4.2 2-D comb function.....	40
4.3 The diffraction order of grating.....	41
4.4 Schematics diagram of the experimental setup.....	45
4.5 Roseta pattern.....	46
4.6 The approximated ring wavelet filter.....	47
4.7 Output of the multi-channel WT output.....	49
4.8 One segment of the single WT output.....	50

Chapter I

Introduction

1.1 Introduction

The *wavelet transform* (WT) is a relatively new concept of signal transformation. The WT has become the subject of considerable theoretical and practical developments in a wide variety of science and engineering fields such as turbulent flow, data compression, signal representation, fingerprint recognition, speech analysis, image processing etc (Hubbard, 1995). The WT, an extension of Fourier analysis, is used to overcome a problem of simultaneous time/space-frequency representation of non-stationary signals. In the field of signal processing, a method for analyzing non-stationary signals by using a WT is of principal interest because use of the WT provides a multi resolution joint time/space-frequency signal representation.

1.2 Historical Review

The WT can be computed by using either digital or optical processing. In comparison with the optical processing, the digital calculation of the WT is relatively slow, especially when we deal with two-dimensional (2-D) signals. On the other hand, optical processing techniques provide a simple and effective

approach for implementing the WT for signal representations. In the field of optics, the implementation of the WT can be easily done by using a well known 4-f optical setup (Lu, et al., 1992). The optical wavelet transformation's concept was first introduced in 1982 by Freysz et al., in order to analyze fractal aggregates (Hubbard, 1995). Later several optical WTs have been reported by different research groups (Szu, Sheng and Chen, 1992; Medlovic and Konfoti, 1993; Mendlovic, Ouxieli, Kiryushev and Marom, 1995; Sheng, Lu, Roberge and Caulfield.,1992; Sheng, Roberge and Szu, 1992; Lu et al., 1992; Zalevsky 1998; Widjaja, 1999).

According to the work of Sheng et al., (1992), optical implementation of the 1-D WT was accomplished by using a bank of wavelet filters. The wavelet filter was made of an optical transmittance mask. In order to compute simultaneously the multi-resolution signal analysis, a bank of wavelet filters was constructed by stacking several 1-D wavelet filters with different dilation in vertical direction. The 2-D optical implementation of the WT by using a computer generated multi-reference matched filter and Dammann grating has been reported by Mendlovic et al., in 1995. The Dammann grating was used for replicating a spectrum of the input pattern into separate channels. By using a conventional VanderLugt correlator (Goodman, 1996) and a multi-reference daughter wavelet synthesized as matched filter, each daughter wavelet was processed separately. At the output plane, a set of WTs was spatially multiplexed and simultaneously displayed in real time. However, this

approach required an accurate alignment of a reference beam used for encoding the daughter wavelet.

In order to avoid the problem of alignment of the matched filter, the implementation of a continuous 2-D on-axis optical WT by using white light source has been proposed by Zeev Zalevsky in 1998. In this method, the white light source was used as an illuminating light source. The WT was performed by taking advantage of the nature of the Fourier optics where the spectrum size of the input image is inversely proportional to the wavelength of the illuminating light. Since only the mother wavelet is used, there is no problem of overlapping between the WT output of different daughter wavelets. Although this proposed method could perform the WT of 2-D signals, but the multi resolution analysis could only be achieved by putting sequentially different color filters in the output plane.

Widjaja, J. (1999) has suggested a different method for implementing the multi channel 2-D WT. In this method, the multiple images of the input scene were first generated by using a binary phase grating. The multi-channel 2-D WT was then performed in parallel by using a holographic lens array. Although this method can generate a real time 2-D optical WT, but the fabrication of the holographic lens array may not be easily done.

1.3 Purpose of the thesis

The purpose of this thesis is to study the optical implementation of the multi channel 2-D WT by using wavelength multiplexing. The idea behind this

study is to combine the method for generation of multiple images of the input scene (Widjaja, 1999) and the use of white light source (Zalvesky, 1998). The wavelength multiplexing can be easily done by using polychromatic light source. Due to unavailability of the white light source, in our proposed method, a combination of the coherent light sources is constructed to obtain the wavelength multiplexing. Our setup consists of two cascaded 4-f optical setups. The first setup is used for producing the multiple images, while the second one is for performing the multi channel 2-D WT. To obtain the multi resolution analysis, multi color filters correspond to the desired wavelength scales are used at the output plane.

1.4 Hypothesis

According to Fourier optics, multi-channel processing can be realized by using the 4-f optical setup as follows: The input pattern to be replicated is placed on the object plane. By putting a grating at the Fourier plane, multiple images of the input pattern can be generated at the output plane. Therefore, by cascading two 4-f optical setups, the first for the multiple imaging and the second for the correlation operation, the multi-channel optical correlation could be implemented. Finally, if the wavelength of the illumination light source is multiplexed then a multi-channel 2-D optical WT could be performed. The WT output produced by a scaling with a shorter wavelength consists of high spatial frequency components, while as for the longer

wavelength the resultant output consists of lower spatial frequency component.

1.5 Organization of the thesis

Chapter 1 of this thesis presents the background of this research work where the optical implementation of the 2-D WT by using wavelength multiplexing is studied.

Chapter 2 discusses the WT 's philosophy, its definition and properties. A Morlet wavelet, a widely used wavelet function, will be introduced. An effect of the scaling factor on the wavelet is illustrated by using the Morlet wavelet.

Chapter 3 discusses the fundamentals of the Fourier optics. The discussion starts with a Fourier transform (FT) and its important properties. The FT properties of thin lenses and the coherent optical processing with spatial filtering will be presented.

Chapter 4 the main part of this study: the optical implementation of the 2-D WT by using wavelength multiplexing. Mathematical analysis of the proposed method will be first presented and then followed by the experimental verifications. The experimental results will be analyzed and compared with the computer simulations. The system performance will also be evaluated.

Chapter 5 summarizes the thesis.

Chapter II

Wavelet Transform

2.1 Why the Wavelet Transform ?

Mathematical transformations are used in the analysis of signals in order to obtain a further information from the original signal that is not readily available in its raw format. For example, when we plot a time-domain signal we will obtain a temporal amplitude representation of the signal. This representation is not always the best representation of the signal because some information is hidden in the frequency content of the signal. In many cases of signal analysis, the frequency spectrum of the signal plays an important role. The frequency content of the signal can be analyzed by using the *Fourier transform* (FT). The FT is a reversible transformation that transforms the time-amplitude representation of a signal into the frequency-amplitude representation and its reverse as shown in Fig. 2.1. The FT of a time signal $x(t)$ is defined by (Papoulis, 1962)

$$X(f) = \int_{-\infty}^{\infty} x(t) \exp(-j2\pi ft) dt, \quad (2.1)$$

while its inverse FT is given by

$$x(t) = \int_{-\infty}^{\infty} X(f) \exp(j2\pi ft) df. \quad (2.2)$$

The FT gives frequency information of the signal by providing which frequency

exists in the signal but does not reveal when this frequency occurs. This can be clearly seen from Figs 2.2 and 2.3. Figures 2.2(a) and 2.3(a) show the stationary cosine signal $x_1(t)$ and the non-stationary cosine signal $x_2(t)$, respectively.

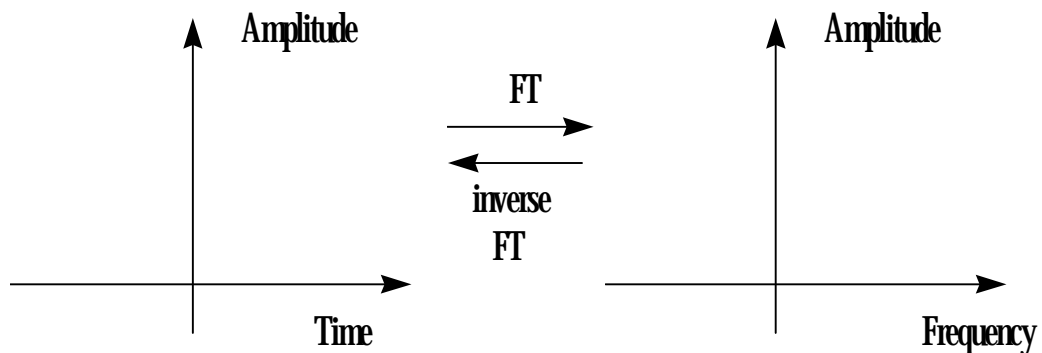


Fig. 2.1 Relationship between the FT and its inverse FT

The stationary signal $x_1(t)$ having two frequency components of 1 Hz and 10 Hz all time can be mathematically represented as

$$x_1(t) = \cos(2\pi t) + \cos(2\pi 10t) .$$

The non-stationary signal $x_2(t)$ also consists of the same two frequency components but these components do not exist all the time. They occur at different times as the following:

$$x_2(t) = \begin{cases} \cos(2\pi t) & ; 0 < t \leq 1000 \text{ms} \\ \cos(2\pi 10t) & ; 1000 \text{ms} < t \leq 2000 \text{ms} \end{cases}$$

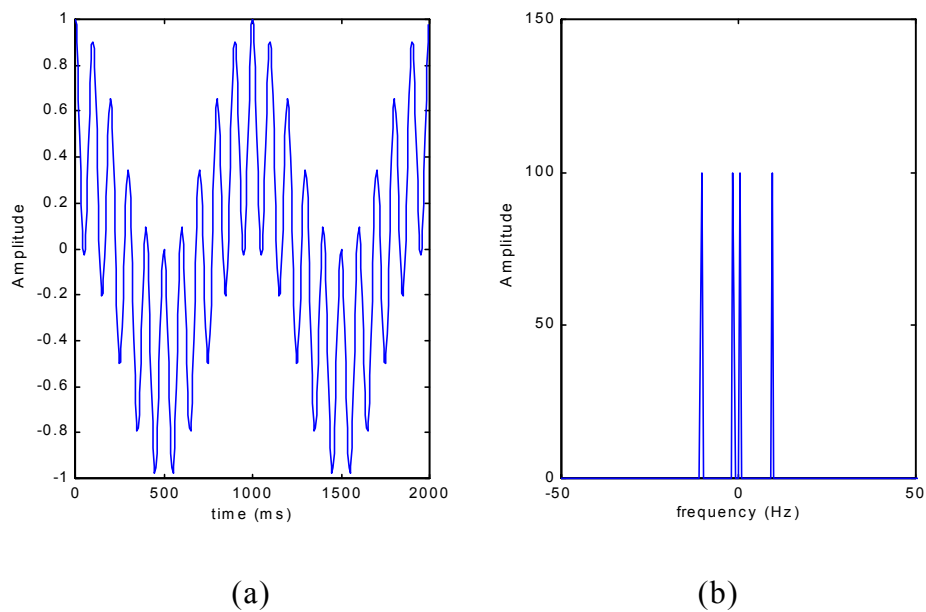


Fig. 2.2 A stationary cosine signal $x_1(t)$ (a) in time domain and (b) its spectrum

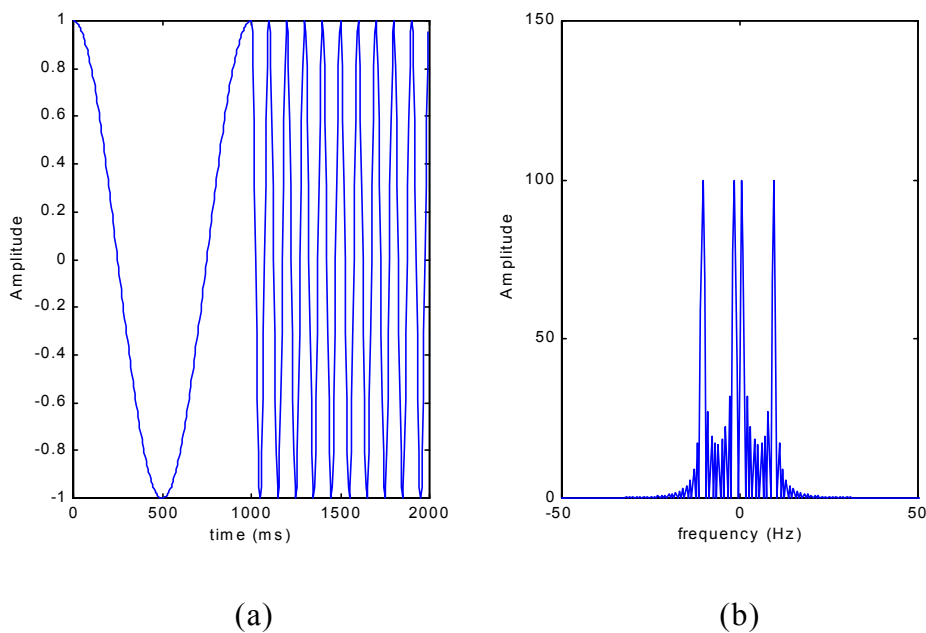


Fig. 2.3 A non-stationary cosine signal $x_2(t)$ (a) in time domain and (b) its spectrum

Although $x_1(t)$ and $x_2(t)$ are two different time signals, but their FTs shown in Fig. 2.2(b) and 2.3(b) give the same frequency information of 1 and 10 Hz, where the noise between the peaks in Fig.2.3(b) coming from the nature of the non-stationary could be neglected. Thus the FT cannot provide time frequency information simultaneously. Note that the graph of the Fourier spectrum is symmetric with respect to the midline of the frequency axis due to the symmetric property of the FT of a real signal.

However, in many cases of signal analysis, non-stationary signals whose frequencies vary with time need to be frequently analyzed. The short time Fourier Transform (STFT) has been developed to solve this problem. The basic concept of the STFT is to analyze small portions of the non-stationary signal which are assumed stationary one at a time. This is performed by multiplying the small portion of the signal by a window function. The resulting product is then Fourier transformed in order to obtain its spectrum. The next step is to shift this window function to the next portion of the signal and again take the FT of the product between the signal and the window function. The process continues until the end of the signal is reached. This will give simultaneously time/space-frequency representation of the entire signal. The STFT of the analyzed signal $x(t)$ can be mathematically expressed as (Burrus, 1998)

$$STFT_x^w(t', f) = \int_{-\infty}^{\infty} x(t)w^*(t-t') \exp(-j2\pi ft) dt, \quad (2.3)$$

where $w(t)$ and t' are the window function and the time shift parameter, respectively. Equation (2.3) shows that the STFT is the FT of the signal multiplied by the shifted window function.

Although the STFT can represent time/space and frequency information simultaneously, it has a resolution problem, since the width of the window function is fixed once it is chosen. Thus the STFT has a fixed resolution at all the time. According to the Heisenberg uncertainty principle (Mallat, 1997), the accuracy of time resolution will decrease when the accuracy of frequency resolution is increased. Therefore, one cannot obtain accurately both time and frequency information at once at arbitrary accuracies. Figures 2.4(a) and (b) show time and frequency resolution of the narrow and the wide window functions, respectively. The narrow window function gives a good time resolution and poor frequency resolution, while the wide window produces poor time resolution but good frequency resolution.

In order to overcome the above limitations of the STFT, a multi-resolution signal analysis by using the WT was developed. The WT is a method for analyzing non-stationary signals with variable resolution as shown in Fig. 2.5. The WT gives good time resolution and poor frequency resolution at high frequencies, while it gives good frequency resolution but poor time resolution at low frequencies. We define the wavelet transform in the next section.

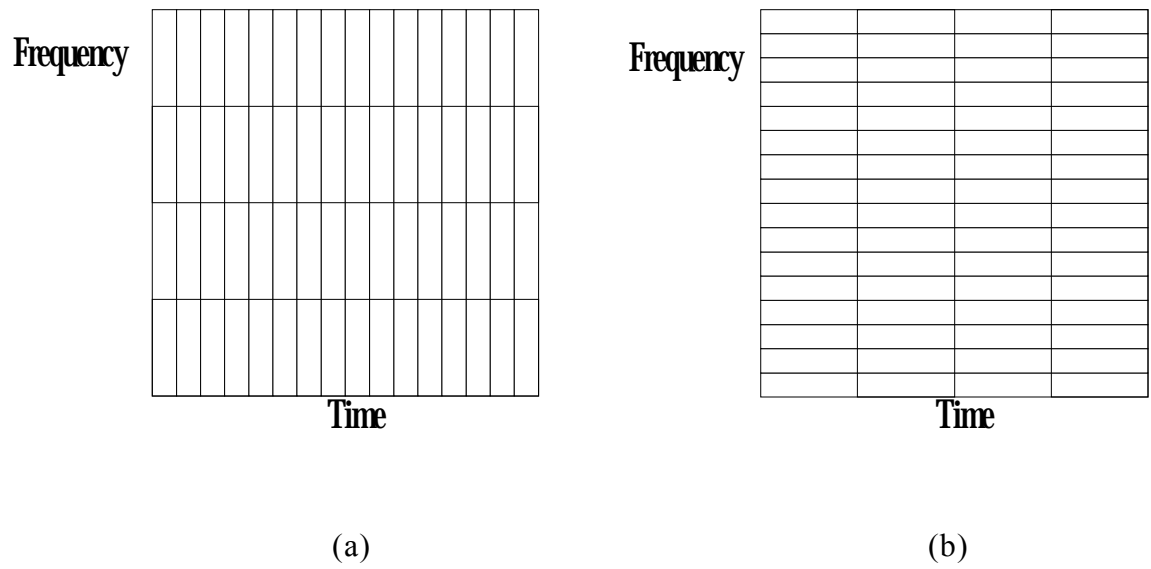


Fig 2.4 Time-frequency plane of STFT for (a) narrow and (b) wide windows (Burrus et al., 1998)

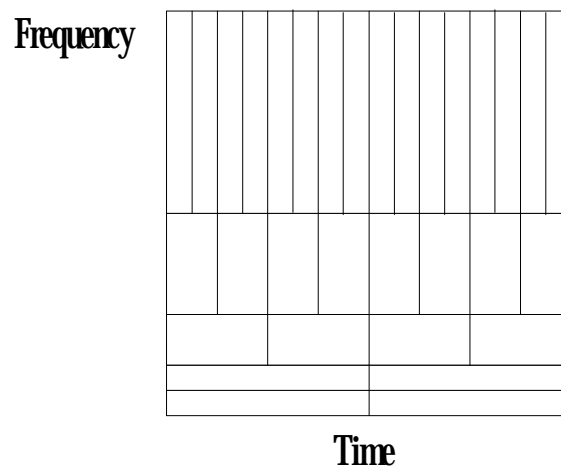


Fig. 2.5 Time-Frequency plane of the WT (Burrus et al., 1998)

2.2 Definition of Wavelet Transform

For image processing purposes, the 2-D spatial signal $f(x,y)$ is frequently used and its WT is defined as (Burrus et al., 1998)

$$W_f(a_x, a_y, b_x, b_y) = \int_{-\infty}^{\infty} \int_{-\infty}^{\infty} f(x, y) h_{a_x a_y b_x b_y}^*(x, y) dx dy, \quad (2.4)$$

where a_x and a_y are the scaling factors along the horizontal and vertical directions, respectively, while b_x and b_y are the translation parameters along the horizontal and vertical directions, respectively. Here $h_{a_x a_y b_x b_y}^*(x, y)$ is the complex conjugate of the daughter wavelet derived from the mother wavelet $h(x, y)$ by dilation and translation:

$$h_{a_x a_y b_x b_y}(x, y) = \frac{1}{\sqrt{a_x a_y}} h\left(\frac{x - b_x}{a_x}, \frac{y - b_y}{a_y}\right). \quad (2.5)$$

Equation (2.4) shows that the WT can be seen as taking the correlation between the original signal $f(x, y)$ and the daughter wavelet function $h_{a_x a_y b_x b_y}(x, y)$. In many cases, a symmetrical scaling factor $a = a_x = a_y$ is widely used. By using the symmetrical scaling factor Eq. (2.5) becomes

$$h_{a b_x b_y}(x, y) = \frac{1}{a} h\left(\frac{x - b_x}{a}, \frac{y - b_y}{a}\right). \quad (2.6)$$

According to Eq. (2.6), when $a < 1$, the mother wavelet $h(x, y)$ is compressed, while $a > 1$ gives a dilation operation. The factor $1/a$ corresponds to the normalization factor. In frequency domain, the WT can be written as

$$W_f(a, b_x, b_y) = a \int_{-\infty}^{\infty} \int_{-\infty}^{\infty} F(u, v) H^*(au, av) \exp\{j2\pi(b_x u + b_y v)\} dudv, \quad (2.7)$$

where $F(u, v)$ and $H^*(au, av)$ are the FTs of $f(x, y)$ and the daughter wavelet, respectively.

2.3 The Morlet Wavelet

The field of signal processing widely uses the Morlet wavelet. The Morlet wavelet was developed by Jean Morlet, a geophysicist with the French oil company Elf-Aquitaine, as a tool for oil prospecting (Hubbard, 1995). It is a cos-Gaussian function (Mendlovic et al., 1995)

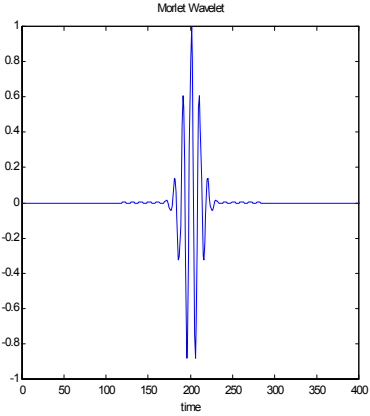
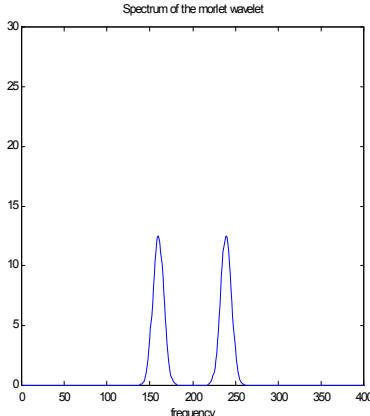
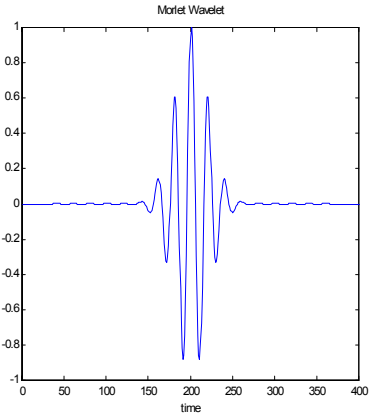
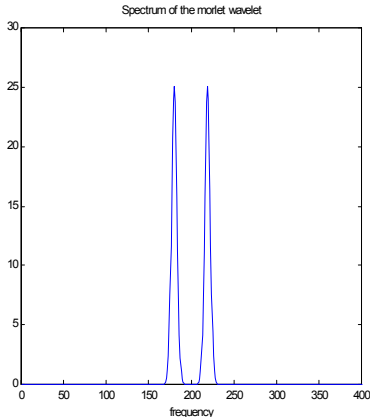
$$h(x, y) = \cos[2\pi f_0 (x^2 + y^2)^{1/2}] \exp\left(-\frac{(x^2 + y^2)}{2}\right), \quad (2.8)$$

where f_0 is the center frequency of the wavelet. The Fourier spectrum of the Morlet wavelet can be written as

$$H(u, v) = 2\pi \exp\{-2\pi^2[(u^2 + v^2)^{1/2} - f_0]^2\}. \quad (2.9)$$

Table 2.1 illustrates the effect of the scaling factor in spatial/time and frequency domain of the Morlet wavelet. The use of a small scale produces a narrow width of the window function, while a large scale gives a wider width of the function. In the frequency domain, the effect of scaling can be explained as follows: According to the property of the FT, the narrow width of window caused by the small scaling parameter provides a higher frequency response in comparison with the use of the larger scaling parameter. We can see that the peak of the both spectra in table 2.1 are not the same, depending on the normalization constant $1/a$ in Eq. (2.6), in such a way that when the wavelet function is compressed, its height will be lower in comparison with the dilated version.

Table 2.1 Morlet wavelet and its spectrum

Scaling	Morlet wavelet	Spectrum of Morlet wavelet
Small	 <p>Morlet Wavelet</p> <p>The plot shows a wavelet signal centered at time 200. The x-axis is labeled 'time' and ranges from 0 to 400. The y-axis ranges from -1 to 1. The signal is a high-frequency oscillation with a peak amplitude of approximately 1.0 and a trough of approximately -0.9.</p>	 <p>Spectrum of the morlet wavelet</p> <p>The plot shows the frequency spectrum of the Morlet wavelet. The x-axis is labeled 'frequency' and ranges from 0 to 400. The y-axis ranges from 0 to 30. There are two distinct peaks: one at approximately 170 Hz with a height of about 13, and another at approximately 230 Hz with a height of about 13.</p>
Large	 <p>Morlet Wavelet</p> <p>The plot shows a wavelet signal centered at time 200. The x-axis is labeled 'time' and ranges from 0 to 400. The y-axis ranges from -1 to 1. The signal is a lower-frequency oscillation with a peak amplitude of approximately 1.0 and a trough of approximately -0.9.</p>	 <p>Spectrum of the morlet wavelet</p> <p>The plot shows the frequency spectrum of the Morlet wavelet. The x-axis is labeled 'frequency' and ranges from 0 to 400. The y-axis ranges from 0 to 30. There are two distinct peaks: one at approximately 170 Hz with a height of about 25, and another at approximately 230 Hz with a height of about 25.</p>

Chapter III

Fourier Optics

3.1 Introduction

Fourier optics is widely used for processing of 2-D optical data or images. In Fourier optics, the principal components of optical processors are often a combination of several thin lenses and a light source where the FT is spatially performed by each thin lens. The optical signal processors can be either coherent or incoherent, depending on the type of source used. Recently many scientists are interested in using optical processing because it can perform parallel processor and achieving 3-D interconnection.

The concept of the optical processor is based on the diffraction effect, caused by the deviation of propagated light beam from its predicted geometrical optics (Jenkins and White, 1976). There are two distinct types of diffraction: Fraunhofer and Fresnel. The Fraunhofer diffraction is used when the distance of a light source from the diffracting aperture and the distance between the observation plane and the aperture are effectively infinite, while the Fresnel diffraction is used when these distances are finite (Jenkins and White, 1976). In both cases, the field distribution in any position must be derived by using the diffraction theory.

The coherent optical processor can be performed by using a well known 4-f optical setup (Goodman, 1996). The spatial filtering can be performed by inserting a spatial filter in the Fourier plane of the 4-f optical setup. Stops and slits are typical example of such filters. The transmittance of stops and slit represent zero and unity, respectively (Karim, 1990).

3.2 Fourier Analysis in Two Dimensions

3.2.1 Definition

In Section 2.1, the FT has been defined for the 1-D signals. However in the field of optics and image analysis, we deal mostly with the 2-D spatial patterns. Therefore, in order to have a better understanding of our study, it is important to define mathematically the FT of the 2-D pattern $f(x,y)$ as (Goodman, 1996)

$$F(f_x, f_y) = \int_{-\infty}^{\infty} \int_{-\infty}^{\infty} f(x, y) \exp[-j2\pi(f_x x + f_y y)] dx dy . \quad (3.1)$$

Its inverse FT can be written as

$$f(x, y) = \int_{-\infty}^{\infty} \int_{-\infty}^{\infty} F(f_x, f_y) \exp[j2\pi(f_x x + f_y y)] df_x df_y . \quad (3.2)$$

Here, f_x and f_y are the number of waves per unit length or the spatial frequencies in the x and y directions, respectively.

3.2.2 Fourier transform theorems

In this section, the basic properties of the FT are reviewed as follows:

3.2.2.1. Linearity theorem.

$$F\{\alpha g + \beta h\} = \alpha F\{g\} + \beta F\{h\}. \quad (3.3)$$

Equation (3.3) shows the FT of a weighted sum of two or more functions, can be simply found by the identically weighted sum of their individual transforms. Here, the symbol "F" denotes the FT operator.

3.2.2.2. Similarity theorem. If $F\{g(x, y)\} = G(f_x, f_y)$, then

$$F\{g(ax, by)\} = \frac{1}{|ab|} G\left(\frac{f_x}{a}, \frac{f_y}{b}\right). \quad (3.4)$$

This theorem shows that a scaling of the signal $g(x, y)$ in the space domain results in an inverse scaling in the frequency domain, and also changes the amplitude of the spectrum.

3.2.2.3. Shift theorem. If $F\{g(x, y)\} = G(f_x, f_y)$, then

$$F\{g(x-a, y-b)\} = G(f_x, f_y) \exp[-j2\pi(f_x a + f_y b)]. \quad (3.5)$$

Equation (3.5) shows that a translation in the space domain gives a linear phase factor in the frequency domain.

3.2.2.4. Rayleigh ' s theorem (Parseval ' s theorem). If F

$\{g(x, y)\} = G(f_x, f_y)$, then

$$\int_{-\infty}^{\infty} \int_{-\infty}^{\infty} |g(x, y)|^2 dx dy = \int_{-\infty}^{\infty} \int_{-\infty}^{\infty} |G(f_x, f_y)|^2 df_x df_y. \quad (3.6)$$

This theorem shows that the energy contain in the signal $g(x, y)$ represented by the integration on the left term is equal to the energy density in the frequency domain on the right term.

3.2.2.5. Convolution theorem. If $F\{g(x, y)\} = G(f_x, f_y)$ and $F\{h(x, y)\} = H(f_x, f_y)$, then

$$\begin{aligned} F\left\{\int_{-\infty}^{\infty}\int_{-\infty}^{\infty}g(\xi, \eta)h(x-\xi, y-\eta)d\xi d\eta\right\} &= F\{g(x, y) \otimes h(x, y)\} \\ &= G(f_x, f_y)H(f_x, f_y), \end{aligned} \quad (3.7)$$

where the symbol " \otimes " denotes the convolution operator (Papoulis, 1962). The FT of the convolution of two functions in the space domain is equivalent to the multiplication of the Fourier spectrum of each individual function.

3.2.2.6. Autocorrelation theorem. If $F\{g(x, y)\} = G(f_x, f_y)$, then

$$\begin{aligned} F\left\{\int_{-\infty}^{\infty}\int_{-\infty}^{\infty}g(\xi, \eta)g^*(\xi-x, \eta-y)d\xi d\eta\right\} &= F\{g(x, y) \otimes g^*(-x, -y)\} \\ &= G(f_x, f_y)G^*(f_x, f_y) \\ &= |G(f_x, f_y)|^2. \end{aligned} \quad (3.8)$$

This theorem may be regarded as a special case of the convolution theorem in which $g(x, y)$ and its complex conjugate $g^*(-x, -y)$ are convolved.

3.2.2.7. Cross correlation theorem. If $F\{g(x, y)\} = G(f_x, f_y)$ and $F\{h(x, y)\} = H(f_x, f_y)$, then

$$\begin{aligned}
F \left\{ \int_{-\infty}^{\infty} \int_{-\infty}^{\infty} g(\xi, \eta) h^*(\xi - x, \eta - y) d\xi d\eta \right\} &= F \{ g(x, y) \otimes h^*(-x, -y) \} \\
&= G(f_x, f_y) H^*(f_x, f_y). \tag{3.9}
\end{aligned}$$

We can see that the correlation output can be found by using the convolution operation.

3.2.2.8. Fourier integral theorem. This theorem points out that for each point of continuity of g ,

$$FF^{-1} \{g(x, y)\} = F^{-1}F \{g(x, y)\} = g(x, y). \tag{3.10}$$

This theorem shows the successive transformation and inverse transformation of a function. The expression in the Eq. (3.10) is satisfied for every continuous points, while at a discontinuous point, two successive transforms replace $g(x)$ by the average values of g in a small neighborhood of that point x .

The above theorems are frequently used in order to find solutions of Fourier analysis problems. These basic properties of the FT will also be used for realizing the WT because the WT could be considered as the convolution of the input signal and the wavelet function. The convolution theorem that relates the spatial and frequency domain information is the main technique for performing the optical signal processing and the optical WT. The Fourier integral theorem (3.2.2.8) shows that the FT is a reversible transform. In the

field of optics, the performance of the FT and its inverse can be clearly shown in the 4-f optical setup.

3.3 The Huygens-Fresnel Principle and Diffraction

Theory

In order to find the field distribution under the diffraction theory, the Huygens-Fresnel principle is used (Goodman, 1996). Figure 3.1 shows the geometry for finding the field distribution at the observation point due to a diffracting aperture. Let us assume that the diffracting aperture lies in the plane (ξ, η) with the area size of Σ , while the observation is being made at the plane (x, y) , which is parallel to the (ξ, η) plane at normal distance z from the aperture. The vector position pointing from the observation point P_0 to a point on the diffracting aperture P_1 is represented by \vec{r}_{01} . \vec{n} is the outward normal vector at point P_1 , while θ is the angle between the outward normal \vec{n} and the vector \vec{r}_{01} .

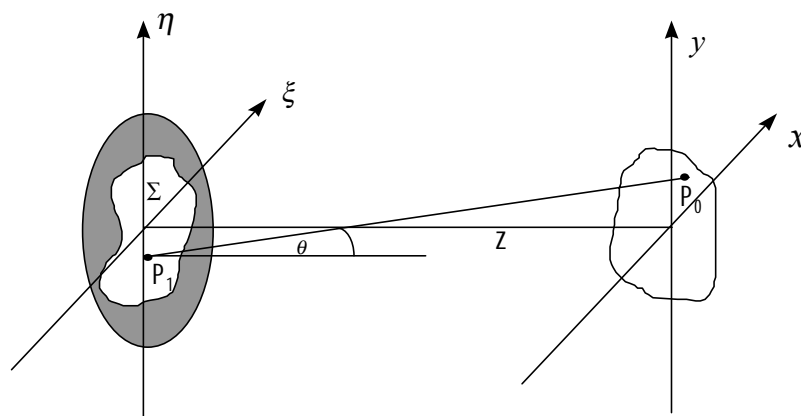


Fig. 3.1 Diffraction geometry

The expression of the field distribution at the observation point $U(P_0)$ in the term of the field distribution at the diffracting aperture $U(P_1)$ is defined as

$$U(P_0) = \frac{1}{j\lambda} \iint_{\Sigma} U(P_1) \frac{\exp(jkr_{01})}{r_{01}} \cos\theta \, ds, \quad (3.11)$$

The distance of the vector \vec{r}_{01} between the observation point and a point in a diffracting aperture can be found by

$$r_{01} = \sqrt{z^2 + (x - \xi)^2 + (y - \eta)^2}. \quad (3.12)$$

From the Fig. 3.1, the term $\cos\theta$ is given by

$$\cos\theta = \frac{z}{r_{01}}, \quad (3.13)$$

therefore the Huygens-Fresnel principle in Eq. (3.11) can be rewritten as

$$U(x, y) = \frac{z}{j\lambda} \iint_{\Sigma} U(\xi, \eta) \frac{\exp(jkr_{01})}{r_{01}^2} d\xi d\eta. \quad (3.14)$$

To reduce the Huygens-Fresnel principle to a more simple and usable expression, the binomial expansion is applied to approximate the distance r_{01} between P_0 and P_1 (Goodman, 1996)

$$r_{01} \approx z \left[1 + \frac{1}{2} \left(\frac{x - \xi}{z} \right)^2 + \frac{1}{2} \left(\frac{y - \eta}{z} \right)^2 \right]. \quad (3.15)$$

By applying the binomial expansion, Eq. (3.14) reduces to

$$U(x, y) = \frac{\exp(jkz)}{j\lambda z} \iint_{-\infty-\infty}^{\infty\infty} U(\xi, \eta) \exp \left\{ j \frac{k}{2z} [(x - \xi)^2 + (y - \eta)^2] \right\} d\xi d\eta. \quad (3.16)$$

The superposition integral is subject to infinite limits due to the boundary conditions and $U(\xi, \eta)$ is nonzero only within the aperture. Eq. (3.16) can be considered as the convolution

$$U(x, y) = \int_{-\infty}^{\infty} \int_{-\infty}^{\infty} U(\xi, \eta) h(x - \xi, y - \eta) d\xi d\eta, \quad (3.17)$$

with the convolution kernel

$$h(x, y) = \frac{\exp(jkz)}{j\lambda z} \exp\left[\frac{jk}{2z}(x^2 + y^2)\right]. \quad (3.18)$$

By expanding these quadratic terms, the field disturbance at point P_0 can thus be expressed as

$$\begin{aligned} U(x, y) = & \frac{\exp(jkz)}{j\lambda z} \exp\left[j\frac{k}{2z}(x^2 + y^2)\right] \int_{-\infty}^{\infty} \int_{-\infty}^{\infty} U(\xi, \eta) \exp\left[j\frac{k}{2z}(\xi^2 + \eta^2)\right] \\ & \times \exp\left[-j\frac{k}{2z}(x\xi + y\eta)\right] d\xi d\eta. \end{aligned} \quad (3.19)$$

If the phase factors outside the integration in Eq. (3.19) are not the main consideration, the field distribution at P_0 can be found by taking the FT of $U(\xi, \eta) \exp[j\pi(\xi^2 + \eta^2)/(\lambda z)]$, provided the spatial frequencies are given by $f_x = x/\lambda z$ and $f_y = y/\lambda z$, respectively, with the wave number $k = 2\pi/\lambda$.

Under the so-called Fresnel approximation, either the source or the observation point is close enough to the diffracting aperture so that the wavefront curvature is not negligible. However there is a second type of diffraction referred to as the Fraunhofer diffraction. It is realized when the distances between the source and the diffracting aperture and between the

aperture and the observation point are both very large (Jenkins and White, 1976). Thus in the Fraunhofer diffraction, the curvature of both the incident and diffracted waves is negligible. The Fraunhofer diffraction is obtained if the condition (Goodman, 1996)

$$z \gg \text{Max} \left[\frac{\pi(\xi^2 + \eta^2)}{\lambda} \right] \quad (3.20)$$

is satisfied. In this case the quadratic phase factor of Eq. (3.19) reduces to unity, thus Eq. (3.19) becomes

$$U(x, y) = \frac{\exp(jkz)}{j\lambda z} \exp \left[j \frac{k}{2f} (x^2 + y^2) \right] \\ \times \int_{-\infty}^{\infty} \int_{-\infty}^{\infty} U(\xi, \eta) \exp[-j2\pi(f_x \xi + f_y \eta)] d\xi d\eta. \quad (3.21)$$

Consequently under the Fraunhofer approximation, the field at P_0 is obtained simply by taking the FT of $U(\xi, \eta)$, and evaluated at spatial frequencies: $f_x = x/\lambda z$ and $f_y = y/\lambda z$. The Fraunhofer diffraction happens to be a special case of the Fresnel diffraction. The analytical expression derived thus can be used to predict the field amplitude distribution across the diffraction pattern for any given aperture. The square of the amplitude can be used as its corresponding intensity distribution. The intensity distribution is more widely used in optical measurements since it corresponds to what would be detected by any detector, including our eyes.

3.4 Fourier Transform Properties of Lenses

It was stated earlier that the lens functions as an important element of the optical data processor. In this section, we concern with the effect of the thin lens on an input optical beam.

3.4.1 The thin lens as phase transformation

The lens is composed of an optically dense material, usually glass with a refractive index of approximately 1.5 (Goodman, 1996), in which the propagation velocity of optical disturbance is less than the velocity in air. The lens is said to be thin if a ray entering at coordinates (x, y) on one face exits at approximately the same coordinates on the opposite face, i.e. if there is negligible translation of a ray within the lens. Thus the thin lens simply delays an incident wave front by an amount proportional to its thickness.

According to Fig. 3.2, Δ_0 represents the maximum thickness of the lens on its axis, while $\Delta(x, y)$ represents the thickness at coordinates (x, y) . The total phase delay introduced by the wave at coordinates (x, y) in passing through the lens may be written as

$$\phi(x, y) = kn\Delta(x, y) + k[\Delta_0 - \Delta(x, y)], \quad (3.22)$$

where n is the refractive index of the lens material. $kn\Delta(x, y)$ and $k[\Delta_0 - \Delta(x, y)]$ are the phase delays introduced by the lens and the region of the free space between the two planes, respectively. The phase transformation of the lens $t_l(x, y)$ can be expressed by

$$t_l(x, y) = \exp[jk\Delta_0] \exp[jk(n-1)\Delta(x, y)]. \quad (3.23)$$

If $U_l(x, y)$ and $U'_l(x, y)$ represent the complex fields incident on a plane immediately in front of the lens and the complex field across a plane immediately behind the lens, respectively, the relationship of these two complex fields can be expressed as

$$U'_l(x, y) = t_l(x, y)U_l(x, y). \quad (3.24)$$

We need to find the mathematical expression of the thickness function $\Delta(x, y)$, in order to see the effect of the lens.

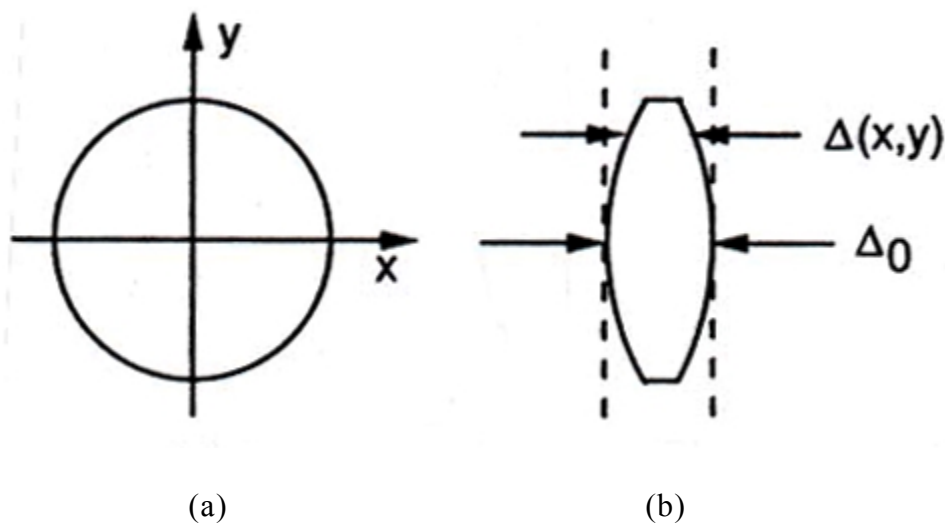


Fig. 3.2 The thickness function. (a) Front view, (b) side view

(Goodman, 1996)

3.4.2 The thickness function

Before specifying the forms of the phase transformations introduced by a many types of lenses, we first define a sign convention: as rays travel from

left to right, each convex surface is taken to have a positive radius of curvature, while each concave surface is taken to have a negative radius of curvature. Thus in Fig. 3.2(b) the radius of curvature of the left-hand surface of the lens is a positive number R_1 , while the radius of curvature of the right-hand surface is a negative number R_2 . To find the thickness $\Delta(x, y)$, the lens is split into three parts, as shown in Fig. 3.3 and the total thickness function can be written as the sum of three individual thickness functions,

$$\Delta(x, y) = \Delta_1(x, y) + \Delta_2(x, y) + \Delta_3(x, y). \quad (3.25)$$

By considering the geometry in Fig. 3.3, the thickness function $\Delta_1(x, y)$ can be written as

$$\begin{aligned} \Delta_1(x, y) &= \Delta_{01} - (R_1 - \sqrt{R_1^2 - x^2 - y^2}) \\ &= \Delta_{01} - R_1 \left(1 - \sqrt{1 - \frac{x^2 + y^2}{R_1^2}} \right). \end{aligned} \quad (3.26)$$

The second component comes from a region of glass of constant thickness Δ_{02} . And the third component is given by

$$\begin{aligned} \Delta_3(x, y) &= \Delta_{03} - (-R_2 + \sqrt{R_2^2 - x^2 - y^2}) \\ &= \Delta_{03} + R_2 \left(1 - \sqrt{1 - \frac{x^2 + y^2}{R_2^2}} \right). \end{aligned} \quad (3.27)$$

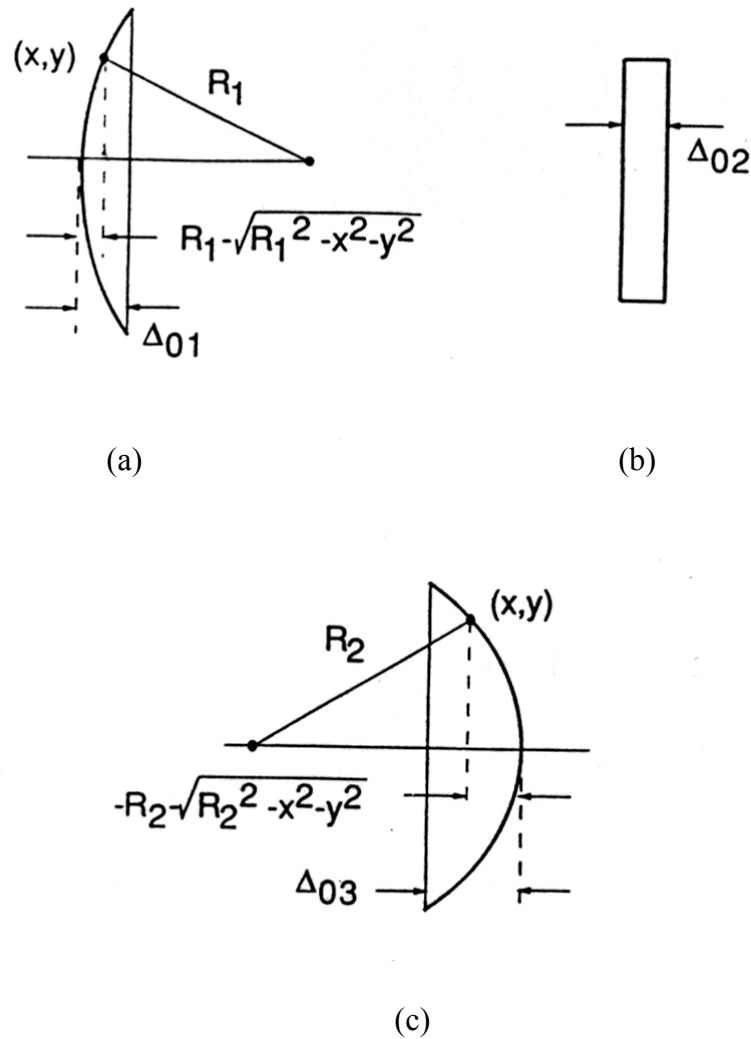


Fig. 3.3 Calculation of the thickness function (a) geometry for Δ_1
 (b) geometry for Δ_2 , (c) geometry for Δ_3 (Goodman, 1968)

Consequently the total thickness $\Delta(x, y)$ can be found by combining the three thickness components as

$$\Delta(x, y) = \Delta_0 - R_1 \left(1 - \sqrt{1 - \frac{x^2 + y^2}{R_1^2}} \right) + R_2 \left(1 - \sqrt{1 - \frac{x^2 + y^2}{R_2^2}} \right) \quad (3.28)$$

where $\Delta_0 = \Delta_{01} + \Delta_{02} + \Delta_{03}$.

3.4.3 The paraxial approximation

The expression of the thickness function can be simplified if analysis is restricted to portions of the wavefront that lie near the lens axis: the paraxial approximation is concerned. Thus we will consider only the values of the coordinates x and y which are sufficiently small to allow the following approximations to be accurate:

$$\sqrt{1 - \frac{x^2 + y^2}{R_1^2}} \approx 1 - \frac{x^2 + y^2}{2R_1^2}. \quad (3.29)$$

$$\sqrt{1 - \frac{x^2 + y^2}{R_2^2}} \approx 1 - \frac{x^2 + y^2}{2R_2^2}. \quad (3.30)$$

In this way, the spherical surfaces of the lens are approximated by parabolic surfaces. Therefore the thickness function becomes

$$\Delta(x, y) = \Delta_0 - \frac{x^2 + y^2}{2} \left(\frac{1}{R_1} - \frac{1}{R_2} \right) \quad (3.31)$$

3.4.4 Phase transformation and its physical meaning

Substitution of Eq. (3.31) into Eq. (3.23) gives the following approximation to the lens transformation:

$$t_l(x, y) = \exp[jkn\Delta_0] \exp \left[-jk(n-1) \frac{x^2 + y^2}{2} \left(\frac{1}{R_1} - \frac{1}{R_2} \right) \right]. \quad (3.32)$$

The physical properties of the lens which consists of the variables n , R_1 and R_2 can be combined in a single number f called the focal length. The focal length of the lens is defined as

$$\frac{1}{f} \equiv (n-1) \left(\frac{1}{R_1} - \frac{1}{R_2} \right). \quad (3.33)$$

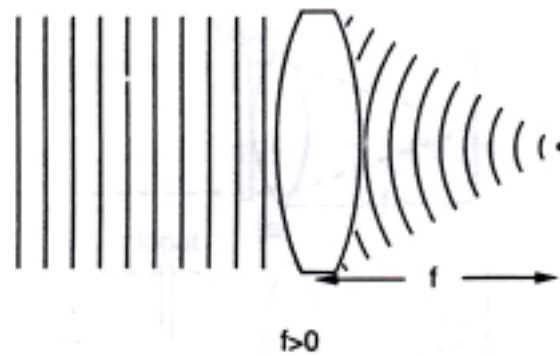
If the constant phase factor is neglected, the phase transformation may be written as

$$t_l(x, y) = \exp \left[-j \frac{k}{2f} (x^2 + y^2) \right]. \quad (3.34)$$

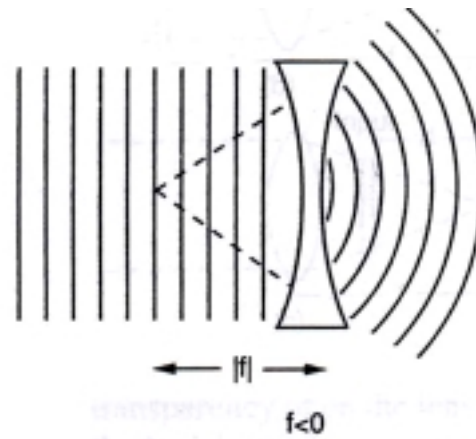
This equation will serve as the basic representation of the effect of a thin lens on an incident optical disturbance. If the field distribution U_l in front of the lens is unity, then a substitution of Eqs. (3.34) into (3.24) yields the following expression for U'_l behind the lens:

$$U'_l(x, y) = \exp \left[-j \frac{k}{2f} (x^2 + y^2) \right]. \quad (3.35)$$

This expression can be interpreted as a quadratic approximation to a spherical wave. If the focal length is positive, then a spherical wave is converging towards a point on the lens axis at a distance f behind the lens, while for a negative focal length, the spherical wave is diverging from a point on the lens axis at a distance f in front of the lens as illustrated in Fig. 3.4. Thus the lens with the positive focal length is called as the positive or converging lens, while the negative focal length is called as the negative or diverging lens.



(a)



(b)

Fig. 3.4 Effects of (a) a converging lens and (b) a diverging lens on a normally incident plane wave (Goodman, 1996)

3.4.5 Fourier transformation by a positive lens

The arrangement for performing the FT operation by using the positive lens is shown in Fig. 3.5. The input transparency having an amplitude transmittance $t_A(x, y)$ is placed a distance d in front of the converging lens with the focal length of f . The input transparency is illuminated by a

monochromatic plane wave of amplitude A . The field distribution transmitted by the input transparency is

$$U_t = At_A. \quad (3.36)$$

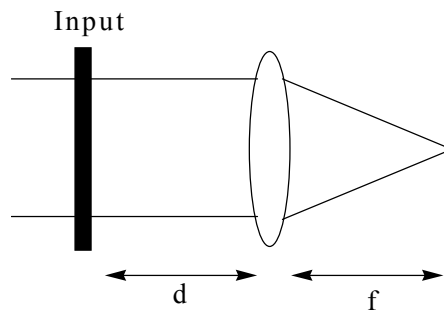


Fig. 3.5 The geometry for performing the Fourier transform by a positive thin lens

Due to the finite extent of a lens can be expressed in terms of the pupil function $P(x, y)$:

$$P(x, y) = \begin{cases} 1 & ; \text{ inside the lens aperture} \\ 0 & ; \text{ otherwise.} \end{cases} \quad (3.7)$$

The derived field distribution is limited on this function. Let $F_0(f_x, f_y)$ represent the Fourier spectrum of the light transmitted by the input transparency, and $F_l(f_x, f_y)$ represents the Fourier spectrum of the light incident on the lens U_l ; that is

$$F_0(f_x, f_y) = F\{At_A\}$$

$$F_l(f_x, f_y) = F\{U_l\}$$

Assuming that the light propagation over distance d is valid for the Fresnel or the paraxial approximation, then relationship between the F_0 and F_l can be expressed as

$$F_l(f_x, f_y) = F_0(f_x, f_y) \exp(jkz) \exp[-j\pi\lambda d(f_x^2 + f_y^2)], \quad (3.38)$$

where the exponential term corresponds to the transfer function of propagation through free space over distance d . If the constant phase factor is dropped, Eq. (3.38) becomes

$$F_l(f_x, f_y) = F_0(f_x, f_y) \exp[-j\pi\lambda d(f_x^2 + f_y^2)]. \quad (3.39)$$

To find the field distribution $U_f(u, v)$ in the back focal plane of the lens, the Fresnel diffraction formula in Eq. (3.19) is used. By neglecting the finite extent of the lens, letting $P = 1$ and setting $z = f$, we obtain

$$U_f(u, v) = \frac{\exp\left[j\frac{k}{2f}(u^2 + v^2)\right]}{j\lambda f} F_l\left(\frac{u}{\lambda f}, \frac{v}{\lambda f}\right), \quad (3.40)$$

where $f_x = u/\lambda f$ and $f_y = v/\lambda f$. By substituting Eq. (3.39) into Eq. (3.40), we have

$$U_f(u, v) = \frac{\exp\left[j\frac{k}{2f}\left(1 - \frac{d}{f}\right)(u^2 + v^2)\right]}{j\lambda f} F_0\left(\frac{u}{\lambda f}, \frac{v}{\lambda f}\right)$$

or

$$U_f(u, v) = \frac{\exp\left[j\frac{k}{2f}\left(1 - \frac{d}{f}\right)(u^2 + v^2)\right]}{j\lambda f}$$

$$\times \iint t_A(x, y) \left[-j \frac{2\pi}{\lambda f} (\xi u + \eta v) \right] d\xi d\eta. \quad (3.41)$$

It is now clear that the distribution of amplitude and phase at the back focal plane (u, v) are again related to the spectrum of the input image. For the special case $d = f$, the quadratic phase factor which precedes the integral vanishes. Evidently when the input image is placed at the front focal plane of the lens, the phase curvature disappears, leaving the exact FT relation as

$$\begin{aligned} U_f(u, v) &= \frac{A}{j\lambda f} \iint_{-\infty-\infty}^{\infty\infty} t_A(\xi, \eta) \exp[-j \frac{2\pi}{\lambda f} (\xi u + \eta v)] d\xi d\eta \\ &= \frac{1}{j\lambda f} F_0 \left(\frac{u}{\lambda f}, \frac{v}{\lambda f} \right) \end{aligned} \quad (3.42)$$

Equation (3.42) shows that the spectrum of the input transparency t_A is actually a function of the wavelength of the illuminating light. By varying the wavelength, scaling of the size of the spectrum could be achieved. Furthermore, in case of a polychromatic light, Eq. (3.42) can be rewritten as

$$\begin{aligned} U_f(u, v) &= \frac{As(\lambda)}{j\lambda f} \iint_{-\infty-\infty}^{\infty\infty} t_A(\xi, \eta) \exp[-j \frac{2\pi}{\lambda f} (\xi u + \eta v)] d\xi d\eta \\ &= \frac{s(\lambda)}{j\lambda f} F_0 \left(\frac{u}{\lambda f}, \frac{v}{\lambda f} \right) \end{aligned} \quad (3.43)$$

where $s(\lambda)$ represents the spectral distribution of the polychromatic light. Thus, multi-scaled spectra of the input transparency can be simultaneously obtained by using the polychromatic light. This interesting characteristic of

the optical FT has been employed by Zeev Zalvesky (1998) for the optical implementation of the 2-D WT.

3.5 Coherent Optical Information Processing System with Spatial Filtering

The performance of the optical system is often characterized by its impulse response. The impulse response can be defined as the output of the system to which an impulse signal is applied. The impulse response function can be used to estimate the output characteristics of the system for every input signal.

Let the impulse response of an optical system be described by $h(x,y)$, where the image plane is in the xy plane. Consider a distributed source that is positioned in the object plane. A distributed source can always be considered as an ensemble of an infinite number of point sources. For simplicity, let the amplitude due to all of these point sources at (ξ,η) be represented by $u_o(\xi,\eta)$. The resultant output field amplitude is obtained by adding the amplitude contributed by all constituent point sources

$$\begin{aligned} u_i(x,y) &= \int_{-\infty}^{\infty} \int_{-\infty}^{\infty} u_o(\xi,\eta) h(x-\xi, y-\eta) d\xi d\eta \\ &= u_o(x,y) \otimes h(x,y). \end{aligned} \tag{3.43}$$

Accordingly, the amplitude of the output image for any input can be determined from the impulse response $h(x, y)$. The output intensity distribution of a coherent optical system is found by

$$I(x, y) = |u_o(x, y) \otimes h(x, y)|^2. \quad (3.44)$$

The FT of the impulse response $H(f_x, f_y)$ is referred as the amplitude transfer function (OTF). By using the convolution property of the FT in Eq. (3.7), Eq. (3.42) can be rewritten as

$$U_i(f_x, f_y) = U_o(f_x, f_y)H(f_x, f_y), \quad (3.45)$$

where $U_i(f_x, f_y)$ and $U_o(f_x, f_y)$ are the FTs of $u_i(x, y)$ and $u_o(x, y)$, respectively. The OTF is thus obtained simply as

$$H(f_x, f_y) = \frac{U_i(f_x, f_y)}{U_o(f_x, f_y)}. \quad (3.46)$$

A spatial frequency filtering is an information processing operation in which certain desired spatial frequencies of an input image are removed or modified by spatial filters placed at the Fourier plane of the optical processor. Consider the coherent optical information processing system as shown in Fig. 3.6, where a coherent beam diverging from a pinhole spatial filter placed at the front focal plane of a lens L_1 beam is collimated. This collimated beam is used to illuminate the input object. A lens L_2 performs the FT of the input image, which is located at its front focal plane. The frequency spectrum of the input appears at the back focal plane of the lens L_2 which is referred as the Fourier plane. The output image is obtained by retransformation the Fourier spectrum by a lens L_3 . Such a system can be referred as the 4-f optical setup

due to the length of the system is equal to four focal lengths. In order to perform the spatial filtering, the spatial filter must be inserted in the Fourier plane. The filtered output image appears at the output plane. The filter can be fabricated either as a real optical transmittance mask or as a holographic matched filter (Mendlovic et al., 1995).

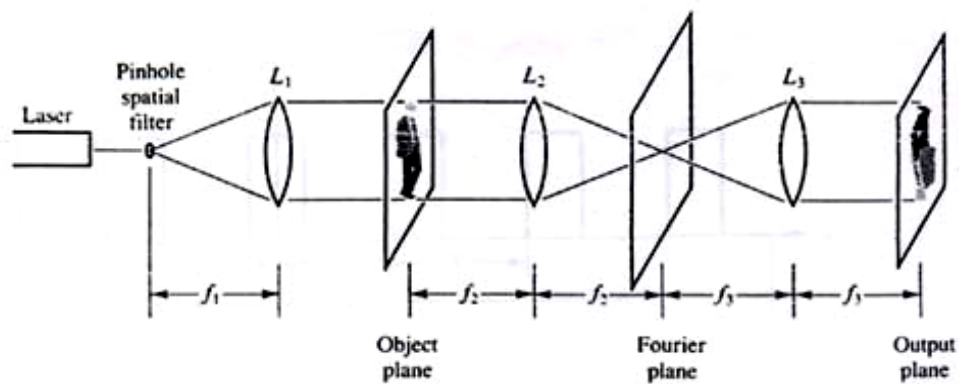


Fig. 3.6 A coherent optical information processing system (Karim, 1990)

Chapter IV

Multi-channel 2-D Optical WT

4.1 Introduction

In Chapter III, it has been shown that the spectrum of any object could be scaled by varying the wavelength of the light source. Our study takes an advantages of this scaling property of the wavelength of light as Zalvesky did. However, our study has a better performance in that the multi-resolution 2-D WT is simultaneously generated. Although automatic variation of the wavelength, the so-called wavelength multiplexing, could be done by the white light source, we instead use the combination of the red and green He-Ne lasers as light sources for experimental verifications since a light source was unavailable during the time this research was being conducted. Two cascaded 4-f optical setups are used for producing multiple images of the input scene to be analyzed and for the multi-channel 2-D WT. In the experiments, the Morlet wavelet and the roseta pattern are used as the analyzing wavelet and the input object, respectively. The experimental results are verified by using Matlab.

4.2 Multi-channel 2-D Optical WT by Using Wavelength Multiplexing

4.2.1 Generation of the multi-channel images by 2-D gratings

Figure 4.1 shows the two cascaded 4-f optical setups. The first setup is used for producing the multiple images, while the second one is for performing the multi-channel 2-D WT. The input object $u_{in}(x_1, y_1)$ placed at a front focal plane of a Fourier transforming lens L1 is illuminated by a collimated light beam having a spectral width $\Delta\lambda$. Its Fourier spectrum $U_{in}(u_1, v_1)$ is diffracted by the 2-D grating positioned immediately behind plane P2.

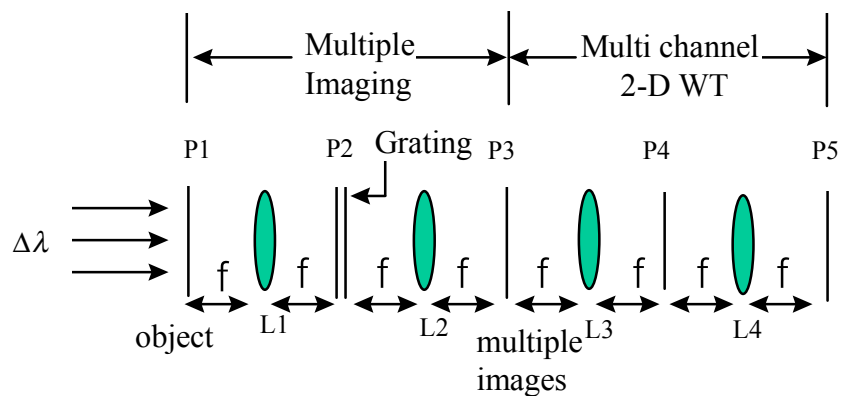


Fig. 4.1 Two cascaded 4-f optical setups

In order to reduce the complexity of the mathematical representation, the sampling theory of the grating is expressed as (Widjaja, 1999)

$$g(u_1, v_1) = \sum_{m=-N}^N \sum_{n=-N}^N \delta(u_1 - m\Delta u_1) \delta(v_1 - n\Delta v_1). \quad (4.1)$$

Here, Δu_1 and Δv_1 are the spatial frequencies of the grating in the horizontal and vertical directions, respectively. The next equation, equation (4.2), represents the 2-D comb function shown in Fig. 4.2. The optical field behind the grating represented by $O(u_1, v_1)$ can be expressed as

$$O(u_1, v_1) = U_{in}(u_1, v_1) \sum_{m=-N}^N \sum_{n=-N}^N \delta(u_1 - m\Delta u_1) \delta(v_1 - n\Delta v_1). \quad (4.2)$$

This may be considered as the product of the Fourier spectrum of the input function $U_{in}(u_1, v_1)$ with the 2-D comb function. By using the Fourier transform property of Eq. (3.7), the multiple images of the original input object are obtained at the plane P3 as

$$\begin{aligned} u'_{in}(x_2, y_2) &= u_{in}(x_2, y_2) \otimes \sum_{m=-N}^N \sum_{n=-N}^N \delta(x_2 - m\Delta x_2) \delta(y_2 - n\Delta y_2) \\ &= \sum_{m=-N}^N \sum_{n=-N}^N u_{in}(x_2 - m\Delta x_2, y_2 - n\Delta y_2). \end{aligned} \quad (4.3)$$

Equation (4.3) shows that the multiple images are generated by the convolution of the original input image with the FT of the 2-D comb function. Here, Δx_2 and Δy_2 corresponding to the distance between centers of the generated images in the horizontal and vertical directions are inversely proportional to Δu_1 and Δv_1 , respectively. This could be explained by considering a general diffraction effect of the 1-D grating shown in Fig. 4.3. The \pm first orders of the diffraction are separated from the zero order term by the distance

$$\Delta x_2 = \lambda z / d, \quad (4.4)$$

where λ and z are the wavelength of the light and the distance between the grating and the observation plane, respectively. d is the spacing of the grating.

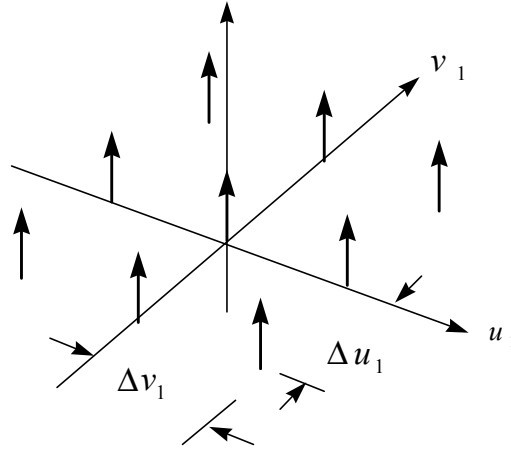


Fig. 4.2 2-D comb function

By taking the grating spacing and the setup into consideration, the distances between the generated images in the horizontal and vertical directions equal to

$$\Delta x_2 = \frac{1}{\Delta u_1} = \lambda f / d \quad (4.5)$$

and

$$\Delta y_2 = \frac{1}{\Delta v_1} = \lambda f / d. \quad (4.6)$$

Therefore Eq. (4.3) can be written as

$$u'_{in}(x_2, y_2) = \sum_{m=-N}^N \sum_{n=-N}^N u_{in}(x_2 - m \frac{\lambda f}{d}, y_2 - n \lambda \frac{\lambda f}{d}). \quad (4.7)$$

It is clear that the position of the resultant multiple images depends on the wavelength of light illumination. The longer wavelength generates wider distance between the zero and the first order of the multiple images in comparison with the shorter one.

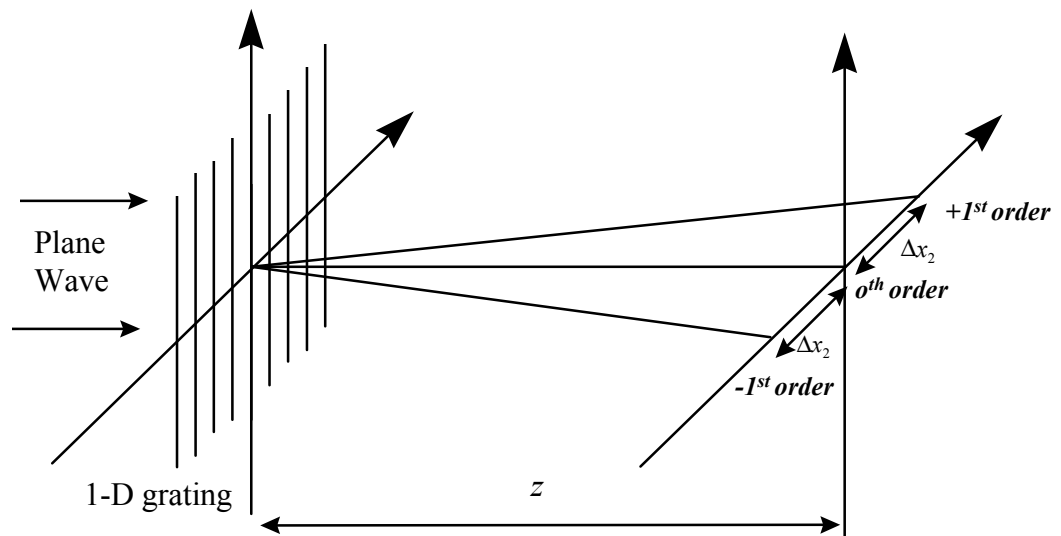


Fig. 4.3 The diffraction order of the grating

4.2.2 Multi-channel WT by using wavelength multiplexing

After the generation of the multiple images by the method described in Section 4.2.1, $u'_{in}(x_2, y_2)$ is Fourier transformed by lens L3. Its generated spectrum can be written as

$$\begin{aligned}
U'_{in}(u_2, v_2) &= \mathcal{F}\{u'_{in}(x_2, y_2)\} \\
&= \mathcal{F}\left\{\sum_{m=-N}^N \sum_{n=-N}^N u_{in}\left(x_2 - m\frac{\lambda f}{d}, y_2 - n\frac{\lambda f}{d}\right)\right\}. \quad (4.8)
\end{aligned}$$

At the back focal plane of L3, the wavelet filter $H(u_2, v_2)$ is inserted, so the optical field at this plane is the multiplication of the spectrum of the multiples images with the wavelet filter as

$$\begin{aligned}
O(u_2, v_2) &= U'_{in}(u_2, v_2)H(u_2, v_2) \\
&= \mathcal{F}\left\{\sum_{m=-N}^N \sum_{n=-N}^N u_{in}\left(x_2 - m\frac{\lambda f}{d}, y_2 - n\frac{\lambda f}{d}\right)\right\}H(u_2, v_2). \quad (4.9)
\end{aligned}$$

By Fourier transforming $O(u_2, v_2)$ using a lens L4, the optical field at the output plane P5 can be expressed as

$$\begin{aligned}
u_{out}(x_3, y_3) &= \mathcal{F}\{U'_{in}(u_2, v_2)H(u_2, v_2)\} \\
&= \sum_{m=-N}^N \sum_{n=-N}^N u_{in}\left(x_3 - m\Delta x_3, y_3 - m\Delta y_3\right) \otimes h\left(\frac{x_3}{\lambda f}, \frac{y_3}{\lambda f}\right). \quad (4.10)
\end{aligned}$$

Equation (4.10) represents the multiple convolution between the input image and the wavelet function which is the multi-channel optical wavelet transforms. In each channel, the WT output can be written as

$$\begin{aligned}
u_{out}(x'_3, y'_3) &= u_{in}(x'_3, y'_3) \otimes h(x_3, y_3) \\
&= \int_{-\infty}^{\infty} \int_{-\infty}^{\infty} u_{in}(x'_3, y'_3) h\left(\frac{b_x - x'_3}{a_x}, \frac{b_y - y'_3}{a_y}\right) dx'_3 dy'_3, \quad (4.11)
\end{aligned}$$

where the coordinate (x'_3, y'_3) represent the position of the WT output in each channel. As for the wavelength multiplexing, the scaling factor of the WT is proportional to the wavelength, then each channel WT output becomes

$$u_{out}(x'_3, y'_3, \lambda) = s(\lambda) \int_{-\infty}^{\infty} \int_{-\infty}^{\infty} u_{in}(x'_3, y'_3) h\left(\frac{b_x - x'_3}{\lambda f}, \frac{b_y - y'_3}{\lambda f}\right) dx'_3 dy'_3, \quad (4.12)$$

for uniform spectral distribution $s(\lambda)$, Eq. (4.12) can rewrite as

$$u_{out}(x'_3, y'_3, \lambda) = \int_{-\infty}^{\infty} \int_{-\infty}^{\infty} u_{in}(x'_3, y'_3) h\left(\frac{b_x - x'_3}{\lambda f}, \frac{b_y - y'_3}{\lambda f}\right) dx'_3 dy'_3, \quad (4.13)$$

and its intensity can be represented as

$$I_{out}(x'_3, y'_3, \lambda) = \left| \int \int u_{in}(x'_3, y'_3) h\left(\frac{b_x - x'_3}{\lambda f}, \frac{b_y - y'_3}{\lambda f}\right) dx'_3 dy'_3 \right|^2. \quad (4.14)$$

4.3 Experimental Setup

Figure 4.4 shows a schematic diagram of the optical setup for implementing multi-channel 2-D optical wavelet transform using wavelength multiplexing. In our setup, the wavelength multiplexing is constructed by combining the red and green He-Ne lasers with the wavelengths equal to 632.8 nm and 543 nm, respectively. The list of the equipment and the instrument is shown in the following:

Equipment

1. Red He-Ne laser , $\lambda = 632.8$ nm
2. Green He-Ne laser, $\lambda = 543$ nm
3. Beam Splitter
4. Reflected mirror
5. Microscope objective of 2.9 mm focal length

6. Achromatic planar convex lenses of 20 cm focal length
7. Roseta pattern with diameter of 7.5 mm
8. 1-D grating 80 lines/mm
9. Wavelet filter with 11 mm inner diameter and 56 mm outer diameter
10. Color filter with bandwidth of 450 nm

Instrument

1. Digital camera [Sony MVC-FD71]

In the experiments, the roseta pattern with the diameter of 7.5 mm object as shown in Fig. 4.5 was used at the input object. The roseta pattern is characterized as having spatial angular frequencies that decrease with the radius (Russ, 1998). It is obvious that the inner part of the roseta pattern has a higher angular spatial frequency in comparison with the outer part. The transparency of a binary approximation of the Morlet wavelet shown in Fig. 4.5 was used as the mother wavelet and was installed at the plane P4. This approximation could be done because the band pass filter may be considered as having a ring-shaped spatial frequency response. In the experiment, the pass band of the wavelet filter is shown in the Table 4.1. The 1-D amplitude grating with 80 lines/mm was aligned along the vertical direction, in order to produce the horizontal multiple images.

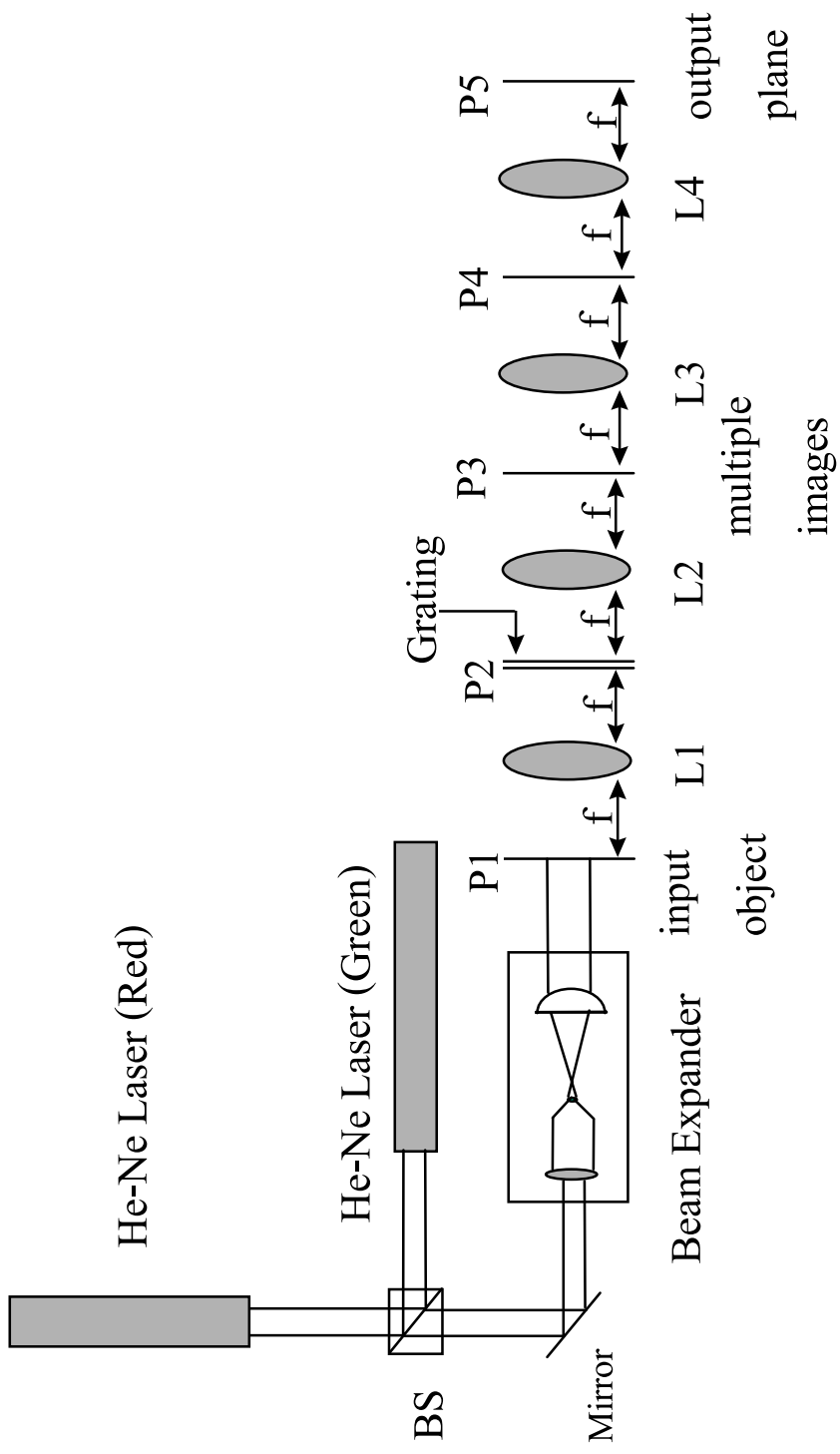


Fig. 4.4 Schematics diagram of the experimental setup

Table 4.1 The pass band of the wavelet filter

Wavelength	Pass band response (lines/mm)
$\lambda=632.8\text{nm}$	8.69~44.25
$\lambda=543\text{ nm}$	10.13~51.56

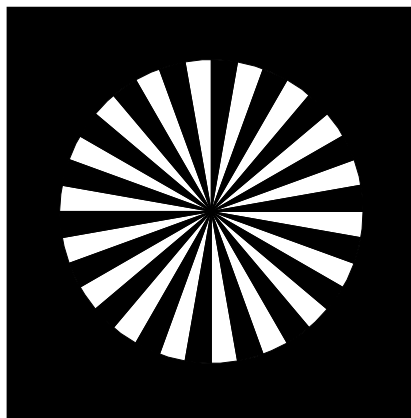


Fig. 4.5 Roseta pattern

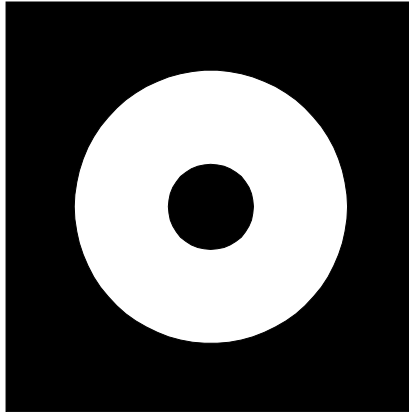


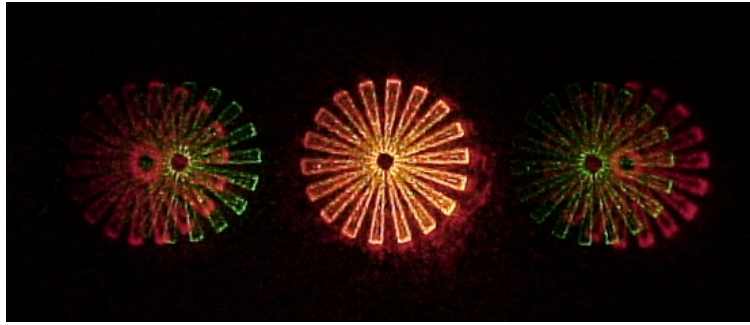
Fig. 4.6 The approximated ring wavelet filter

In order to collimate the light source beam, one set of beam expander based on the Keplerian telescope configuration (Hecht, 1987), consisting of the microscope objective and the planar convex lens with the focal lengths of with 2.9 mm and 38.1 mm, respectively, was used. This produced magnification of 13 times. Four achromatic lenses with the focal length of 200 mm and diameter of 50 mm were used as the Fourier transforming lenses L1, L2, L3, and L4.

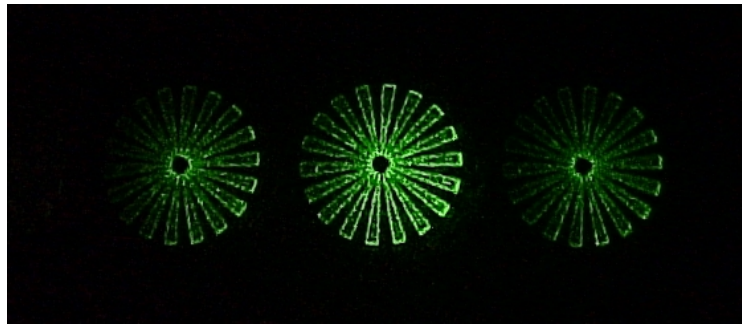
In order to verify the proposed 2-D WT, the output images of the multi-channel optical WT were displayed on the screen. They were captured by the digital camera as a bitmap file with resolution 640×480 pixels. In order to obtain the multi-resolution wavelet analysis, the color filters were placed simultaneously in each channel of the 2-D WT.

4.4 Experimental Results

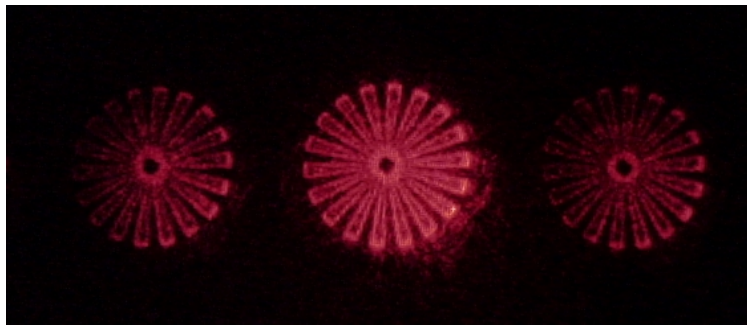
The optical implementation of multi-channel 2-D WT by using wavelength multiplexing was implemented by using the setup as shown in Fig. 4.4. In our experiment three channels of the 2-D WT corresponding to the three diffraction order of the multiple images were produced as the preliminary study. Figures 4.7(a), (b) and (c) show the output images of three channel 2-D WT. Figure 4.7(a) is obtained by multiplexing the red and green laser sources. Figures 4.7(b) and (c) correspond to the images of optical WT when the green and red color filters were used at the output plane, respectively. The generated multiple input scene appeared with a spatial separation Δx_2 of 10.12 mm for 632.8 nm wavelength and 8.69 mm for 543 nm. This spatial separation could be obtained by using Eq. (4.5)



(a)



(b)



(c)

Fig. 4.7 Output of the multi-channel WT (a) for the combination of red and green wavelength (b) for green wavelength (b) for red wavelength.

The captured outputs were rigorously analyzed by scanning their intensity distributions. For simplicity, one segment of the output image of 16×80 pixels as shown in Fig. 4.7 was analyzed. Figure 4.8(a) shows the selected output corresponding to the wavelength of 543 nm, while Fig. 4.8(b) corresponds to the 632.8 nm.

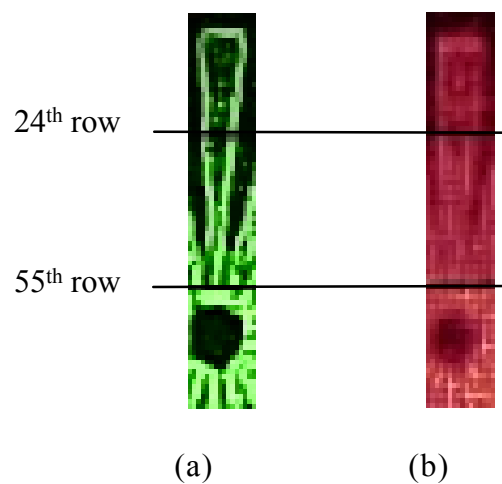


Fig 4.8 One segment of the single channel WT output for wavelength of
(a) 543 nm, and (b) 632.8 nm.

In order to scan the intensity distribution of the output image, the stored bitmap file of the captured image was read into the symbolic program. The scanned intensities were normalized in order to eliminate the different intensity level of the red and green He-Ne lasers. The intensity distributions at the 24th and the 55th rows corresponding to the inner and the outer parts of the wavelet transformed of the roseta pattern were scanned. Figures 4.9 and 4.10 show the scanned intensities on the 24th and 55th rows, respectively. The solid

line corresponds to the scaling by using 543 nm wavelength, while the dash line represents the scaling of 632.8 nm wavelength.

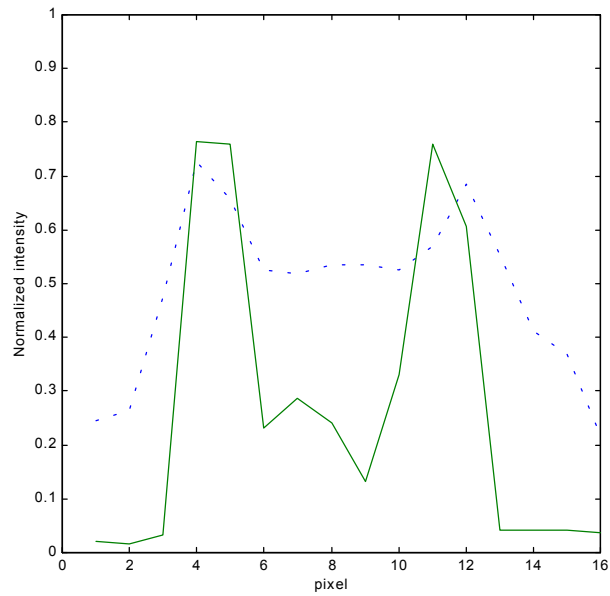


Fig. 4.9 The scanned intensity distribution at 24th row

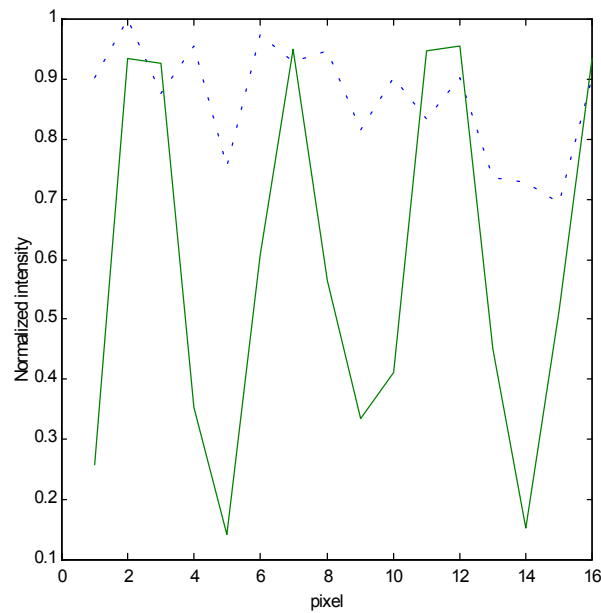


Fig.4.10 The scanned intensity distribution at 55th row

From the scanned intensities and the output images, it can be seen that the WT corresponding to the scaling with 543 nm wavelength gives a stronger edge enhancement in comparison with the 632.8 nm wavelength because the small scaling factor gives the wavelet filter with higher spatial frequency response in comparison with the larger scale. In Fig. 4.9, two peaks corresponding to the both side of the edges of the roseta pattern at 24th row could be seen, while Fig. 4.10 contains four peaks because the inner part of the roseta pattern consists of three segments as shown in Fig. 4.8(a). Furthermore, the normalized intensity at 55th row is higher than the 24th row due to Gaussian characteristic of the laser beam that has a maximum distribution around the optical axis.

The results displayed in Fig 4.7 show that the optical implementation of the multi-channel 2-D WTs was successful. By using an appropriate color filter, the multi-resolution WT analysis can be obtained in real time.

4.5 Computer Simulation.

The edge enhancement effect of the WT was verified by a computer simulation. Since the intensity distribution of one segment of the roseta pattern can be represented the rectangular function, the 1-D simulation was performed. Figure 4.11 shows a flowchart of the simulation which is consisting of 3 computation steps that are:

Step 1: The 1-D rectangular function is generated. The result is plotted as shown in the Fig. 4.12.

Step 2: The Morlet wavelet for a given scaling factor is generated. The results are shown in the Fig. 4.13.

Step 3: The WT of the rectangular function is computed. The resultant outputs are plotted as in the Fig. 4.14.

Although the WT is the correlation between the input function and the wavelet function, for the real and even wavelet function, the correlation output can be calculated by using the convolution operation. In this simulation, the 1-D rectangular function as shown in the Fig. 4.12 was used as an input function. The WT with the scaling factors equal to 1 and 0.86 which is the ratio of green and red wavelength were generated as shown in Fig. 4.13. The simulation results are shown in Fig. 4.14. It is obvious that there are two output peaks corresponding to the edges of the rectangular function in Figs. 4.14(a) and (b). The Morlet wavelet with a smaller scaling factor could be regarded as having higher spatial frequency response in comparison with a longer scaling factor. Therefore, the edge enhancement is stronger. This could be confirmed by Fig. 4.14(b) where the separation between edges is wider.

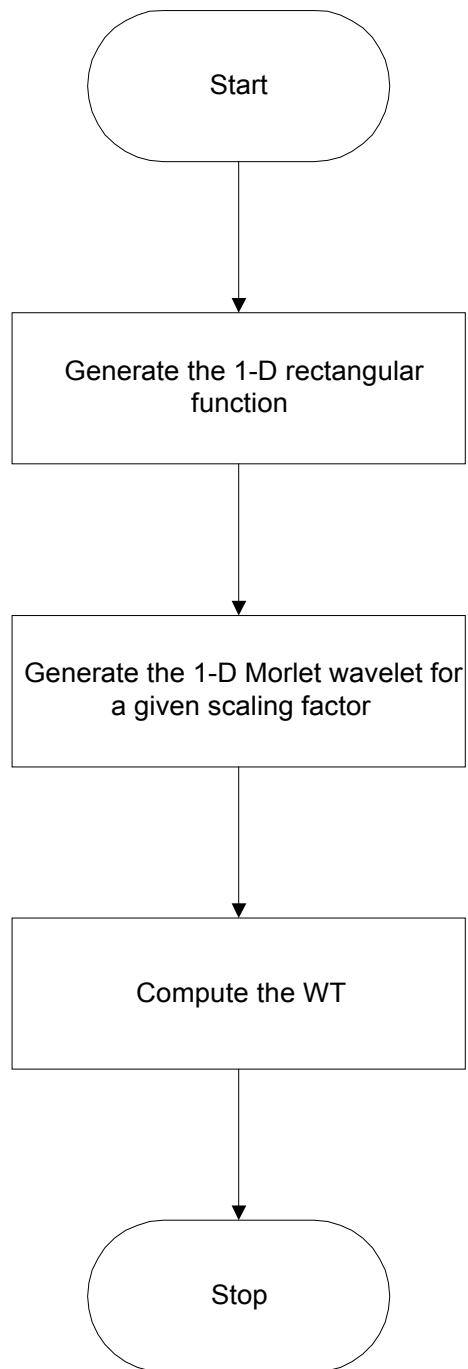


Fig. 4.11 The flowchart of the simulation program

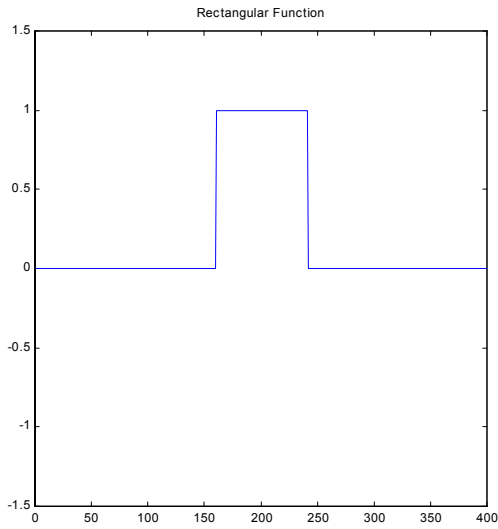


Fig. 4.12 The rectangular function that used as the 1-D input in the simulation

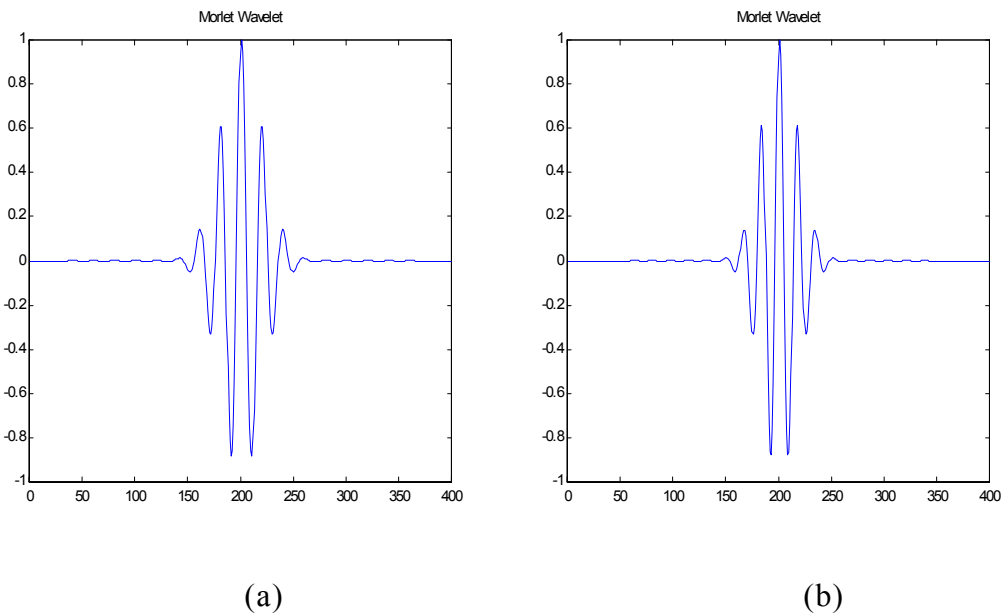


Fig.4.13 The scaled Morlet wavelet (a) for a scaling factor = 1
(b) scaling factor = 0.86

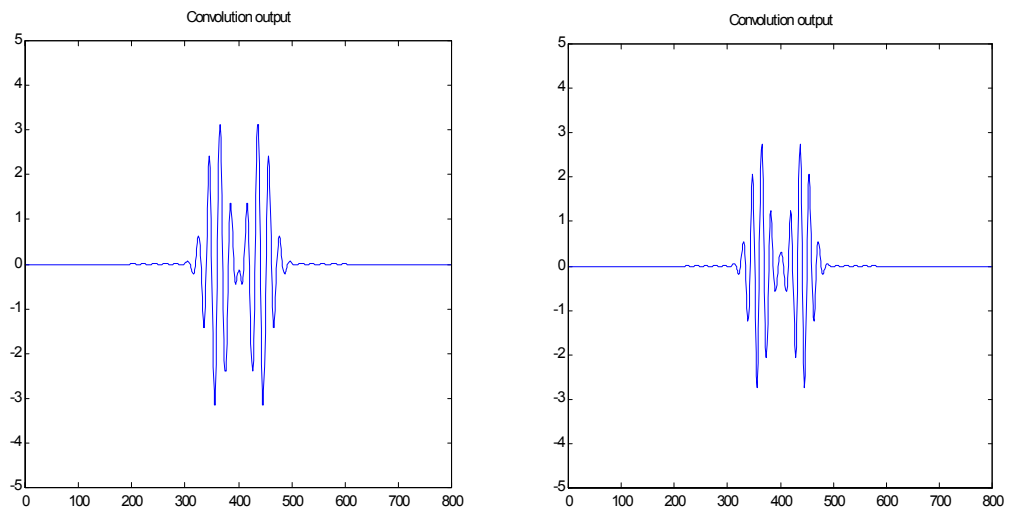


Fig. 4.14 The convolution output (a) corresponding to the 1 scaling factor
(b) corresponding to the 0.86 scaling factor.

As the summary, the experimental results are in a good agreement with the theoretical prediction given by the computer simulation.

4.6 System Performance

In this experiment, the multi-channel 2-D optical WT using wavelength multiplexing was successfully performed in real time. This method can reduce the complexity of implementation of the WT by using only one of the approximated spectrum of the wavelet filter placed on axis in the optical setup.

In our method, the grating plays an important role in generating multiple images. Here, the characteristic of the grating will be analyzed.

In case the input image has a diameter of D , the cross talk between channels could be avoid if the grating used in the system must have minimum spatial frequency of

$$f_{g_{\min}} = \frac{D}{\lambda f}. \quad (4.15)$$

By using this setup with 7.5 mm of the input roseta pattern, the used grating must have minimum spatial frequency equal to 69 lines/mm.

The possibility to extend the number of the channels in this setup without the cross talk problem between each channel could be done by increasing the number of gratings such as crossing the four 1-D grating, oriented in the horizontal, vertical, 45° clockwise, and 45° counter clockwise as shown in Fig. 4.15. As the result, 9 channels of the WT could be produced as shown in Fig. 4.16, where the circular shapes represent the WT output in each channel.

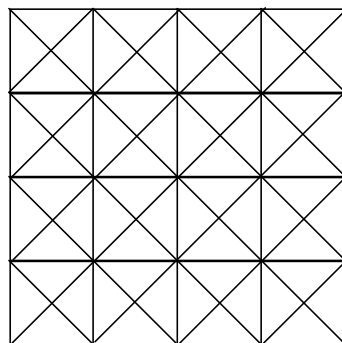


Fig. 4.15 4-crossed gratings with different angular orientation

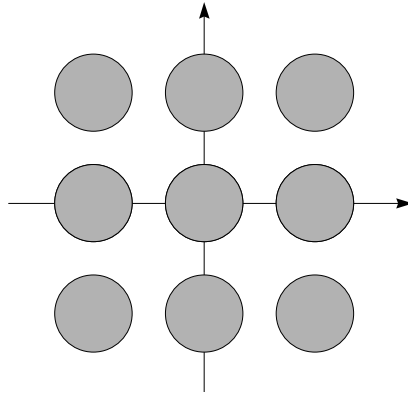


Fig. 4.16 9 channels of the WT output produced by 4-crossed gratings

Chapter V

Conclusion

A new method for implementing the multi-channel 2-D optical WT by using wavelength multiplexing has been proposed and demonstrated. Its system performance has also been evaluated. This method consists of two processes that are the optical generation of the multiple images by using gratings and the second one is simultaneous computation of the multi-channel WT. By wavelength multiplexing, several scaled analyzing wavelet could be generated in parallel from a single wavelet filter. The multi-resolution transformed outputs can be simultaneously obtained by putting the color filter in each channel. Experimental results indicate that the proposed method works in good agreement with the theoretical prediction. By increasing the number of gratings such as crossing four 1-D gratings oriented in the horizontal, vertical, 45° clockwise, and 45° counter clockwise, the number of channels be increased to as many as 9. To avoid cross talk problems between each channel, the used grating must have a minimum spatial frequency of 69 lines/mm.

This study may be extended further in order to obtain finer resolution analysis of the WT by using a white light source. Furthermore, in order to have a real time optical WT, an electrically addressed spatial light modulator (EASLM) could be used to display the wavelet filter. In order to do this, the wavelet filter is first computed and its result is stored in the computer.

The EASLM could be connected to the computer via a hardware interface. By using this EASLM, there is flexibility to modify the wavelet filter in real time.

References

References

- Burrus, C. S., Ramesh, A. and Gau H. (1998). **Introduction to Wavelets and Wavelet Transforms**. New Jersey: Prentice-Hall.
- Goodman, J. W. (1996). **Introduction to Fourier Optics** (2nd ed.). New York: McGraw-Hill.
- Hecht, E. (1987). **Optics** (2nd ed.) MA: Addison-Wesley Pub. Co.
- Hubbard, B. B. (1995). **The World According to the Wavelets**. Wellesley: A K Peters, Ltd.
- Jenkins, A. F., White, E. H. (1976). **Fundamentals of Optics** (4th ed.). New York: McGraw-Hill.
- Karim, A. M. (1990). **Electro Optical Devices and System**. Massachusetts: PWS-KENT Publishing.
- Lu, X. J., Katz, A., Kanterakis, E. G., Li, Y., Zhang Y. and Cavaris, N. P. (1992). Image analysis via optical wavelet transform. **Opt. Commun.** 92:337-345.
- Mallat, S. G. (1997). **A Wavelet Tour of Signal Processing**. MA: Academic Press.
- Mendlovic, D. and Konfoti, N. (1993). Optical realization of the wavelet transform for two-dimensional objects. **Appl. Opt.** 32:6542-6546.

- Mendlovic, D., Ouzieli I., Kiryushev I. and Marom E. (1995) Two-dimensional wavelet transform achieved by computer generated multireference matched filter and Dammann grating. **Appl. Opt.** 34:8213-8219.
- Papoulis, A. (1962). **The Fourier Integral and its Applications**. New York: McGraw-Hill.
- Russ, J. C. (1999). **The Image Processing Handbook** (3rd ed.). Boca Raton, Fla: CRC Press.
- Sheng, Y., Lu, T., Roberge, D. and Caulfield, H. J. (1992) Optical N⁴ implementation of a two-dimensional wavelet transform. **Opt. Eng.** 31:1859-1864.
- Sheng, Y., Roberge D. and Szu, H. H. (1992). Optical wavelet transform. **Opt. Eng.** 31:3267-3277.
- Szu, H., Sheng, Y., and Chen, J. (1992). Wavelet transform as a bank of matched filters. **Appl. Opt.** 31:3267-3277.
- Widjaja, J. (1999). Dynamic optical processing of 2-D wavelet transforms. **Optical Memory and Neural Networks** 8: 75-79.
- Zalevsky, Z. (1998). Experimental implementation of a continuous two-dimensional on-axis optical wavelet transformer with white light illumination. **Opt. Eng.** 37:1372-1375.

Biography

Miss Chanita Kaewprasert was born on 26th August 1977 in Bangkok. She received her Bachelor 's Degree in Telecommunication Engineering from Suranaree University of Technology in 1997. She continued with her graduate studies in the School of Laser Technology and Photonics, Institute of Science, Suranaree University of Technology.